https://doi.org/10.1016/j.ijheatmasstransfer.2018.11.076

Three-dimensional Lattice Boltzmann simulation on thermosolutal convection and entropy generation of Carreau-Yasuda fluids

GH. R. Kefayati [a,*], H. Tang [b]

[a] *School of Engineering, University of Tasmania, Hobart, Tasmania, Australia*

[b] *Department of Mechanical Engineering, The Hong Kong Polytechnic University, Kowloon, Hong Kong*

Abstract

In this paper, three-dimensional thermosolutal natural convection and entropy generation in a cubic cavity filled with a non-Newtonian Carreau-Yasuda fluid has been simulated by Lattice Boltzmann Method (LBM). This study has been conducted for certain pertinent parameters of Rayleigh number (Ra = 10^4 and 10^5), the Buoyancy ratio (N = -1, 0.1, 1), the Lewis number (Le = 0.5, 2.5, 10), power-law indexes (n = 0.5, 1, and 1.5), Carreau number (Cu = 0.01, 0.1, 1, 10 and 100), and Carreau-Yasuda parameter (m = 1, 10, and 100). Results indicate that the rise of Rayleigh number enhances heat and mass transfer for various studied parameters. The increase in power-law index provokes heat and mass transfer to drop gradually. However, the effect of power-law index on heat and mass transfer rises steadily as Rayleigh number rises. The enhancement of Carreau number decreases heat and mass transfer, but; the increases in the Carreau-Yasuda parameter augments heat and mass transfer significantly. The augmentation of the buoyancy ratio number enhances heat and mass transfer. It was found that mass transfer increases as Lewis number augments. The augmentation of Rayleigh number enhances different entropy generations and declines the average Bejan number. The increase in the power-law index provokes various irreversibilities to drop significantly. The enhancement of the buoyancy ratio causes the summation entropy generations to increase considerably. The rise of Carreau number and Carreau-Yasuda parameter decreases and increases the total irreversibilities; respectively.

Key words: Entropy, Carreau-Yasuda fluid, Natural convection, Mass transfer, 3D LBM

* Corresponding author. Dr. Gholamreza Kefayati (GH. R. Kefayati)
Email addresses: gholamrezakefayati@gmail.com, gholamreza.kefayati@utas.edu.au (GH. R. Kefayati), h.tang@polyu.edu.hk

1 Introduction

Natural convection driven by buoyancy due to simultaneous temperature and concentration gradients is generally referred to as double diffusive or thermosolutal convection. Thermosolutal convection occurs in a wide variety of fields such as oceanography, astrophysics, geology and metallurgy. Over the past decades, studies on Newtonian double diffusive convection have been reflected by a number of publications [1–8]. However, in many cited fields, the applied fluids show a non-Newtonian manner. Some limited studies about thermosolutal convection of power-law fluids in a two and three dimensional enclosures have been studied [9,10].
Generally, fluids are classified into two main groups: Newtonian and non-Newtonian fluids. In most fluids without memory, the main difference between Newtonian and non-Newtonian fluids is the relationship between the extra stress tensor ($\boldsymbol{\tau}$) and the deformation rate tensor ($\mathbf{D}$). The constitutive equation of an incompressible Newtonian fluid is written in the following form:

$$\boldsymbol{\tau} = 2\,\eta\,\mathbf{D}\ , \qquad \mathbf{D} = \frac{1}{2}\left(\nabla\mathbf{u} + (\nabla\mathbf{u})^T\right) \tag{1.1}$$

where η is the dynamic viscosity. Eq.(1.1) shows that the extra tensor has a linear relation with the rate of deformation tensor. Carreau fluid is a special sub-class of non-Newtonian fluids in which follows the Carreau model [11]. This model was introduced in 1972 and has been applied extensively up to date. The constitutive equation of an incompressible Carreau fluids is as

$$\boldsymbol{\tau} = 2\,\eta(\dot{\gamma})\ \mathbf{D} \tag{1.2}$$

where

$$\eta(\dot{\gamma}) = \eta_\infty + (\eta_0 - \eta_\infty)\ \left[1 + (\lambda\dot{\gamma})^2\right]^{(n-1)/2}\ , \tag{1.3}$$

where $\dot{\gamma}$ is the equivalent strain rate or the shear rate and defined as

$$\dot{\gamma} = \sqrt{2\,\mathbf{D} : \mathbf{D}} \tag{1.4}$$

This model has been improved by Carreau-Yasuda model [12] where is continuous for all positive rate of deformations.

$$\eta(\dot{\gamma}) = \eta_\infty + (\eta_0 - \eta_\infty)\ \left[1 + (\lambda\dot{\gamma})^m\right]^{(n-1)/m}\ , \tag{1.5}$$

where η_0 and η_∞ are the viscosities corresponding to zero and infinite viscosities, λ is the time constant and n is the power-law index where the deviation of n from unity indicates the degree of deviation from Newtonian behavior. With n$\neq$1, the constitute equation represents pseudoplastic fluid ($0 < n < 1$) and for ($n > 1$) it represents a dilatant fluid, respectively. Note that a Newtonian

(H. Tang).

fluid can be recovered as a special case of the present Carreau fluid by letting n = 1 and/or $\lambda = 0$, and a power-law fluid can be obtained by assuming a large λ. m is the Carreau-Yasuda model parameter. The infinite shear viscosity, η_∞, is generally associated with a breakdown of the fluid, and is frequently significantly smaller ($10^3 - 10^4$ times smaller) than η_0. Carreau–Yasuda models have been employed to simulate various chemicals, molten plastics, slurries, paints, blood, etc.

Some limited isothermal and non-isotermal problems of Carreau/Carreau–Yasuda fluids have been studied. Shamekhi and Sadeghy [13] analyzed lid-driven cavity flow of a purely-viscous non-Newtonian fluid obeying Carreau-Yasuda rheological model numerically using the PIM meshfree method combined with the Characteristic-Based Split-A algorithm. Results were reported for the velocity and pressure profiles at Reynolds numbers as high as 1000 for a non-Newtonian fluid obeying Carreau-Yasuda rheological model. The results showed a strong effect of the fluids non-Newtonian behavior, e.g. its shear-thinning behavior, on the velocity profiles inside an enclosure. In addition, it was demonstrated that the power-law index and time constant dramatically affected the size and the position of the primary vortex inside the cavity. Bouteraa et al. [14] performed a linear and weakly nonlinear analysis of convection in a layer of shear-thinning fluids between two horizontal plates heated from below. The shear-thinning behaviour of the fluid was described by the Carreau model. Analysis of the saturation coefficients at cubic order in the amplitude equations showed that the nature of the bifurcation depends on the rheological properties, i.e. the fluid characteristic time and shear-thinning index. For weakly shear-thinning fluids, the bifurcation was supercritical and the heat transfer coefficient increased, as compared with the Newtonian case. When the shear-thinning character was large enough, the bifurcation was subcritical, pointing out the destabilizing effect of the nonlinearities arising from the rheological law. It was shown that in the supercritical regime, only rolls were stable near onset. Pantokratoras [15] considered the flow of a non-Newtonian, Carreau fluid, directed normally to a horizontal, stationary, circular cylinder. The problem was investigated numerically using the commercial code ANSYS FLUENT with a very large calculation domain in order that the flow could be considered unbounded. It was found that for each Carreau number and each power-law index a critical Reynolds number exists where the wake appears. Below this critical Reynolds number no wake exists. They also mentioned all critical Reynolds numbers rise with increasing power-law index. For shear-thickening fluids the variation of critical Reynolds number is monotonic with Carreau number, that is, as the Carreau number increases that critical Reynolds number increases and the opposite is valid for shearthinning fluids. At low power-law index, the wake length changes nonlinearly with increasing Reynolds number and as the power-law index rises the variation becomes linear. When the Carreau number became higher the drag coefficient of shear-thinning fluids decreased and raised in shear-thickening fluids and this happened for all Reynolds numbers. Shahsavari and McKinley

[16] studied the flow of generalized Newtonian fluids with a rate-dependent viscosity through fibrous media with a focus on developing relationships for evaluating the effective fluid mobility. They conducted a numerical solution of the Cauchy momentum equation with the Carreau or power-law constitutive equations for pressure-driven flow in a fiber bed consisting of a periodic array of cylindrical fibers. While the dimensionless mobility was, in general, a function of the Carreau number and the medium porosity, the results showed that for porosities less than $\epsilon \simeq 0.65$, the dimensionless mobility became independent of the Carreau number and the mobility function exhibited power-law characteristics as a result of the high shear rates at the pore scale. We derived a suitable criterion for determining the flow regime and the transition from a constant viscosity Newtonian responsed to a power-law regime in terms of a new Carreau number rescaled with a dimensionless function which incorporates the medium porosity and the arrangement of fibers. Alloui and Vasseur [17] reported a numerical study of natural convection in a vertical enclosure filled with a non-Newtonian fluid. Thermal boundary conditions of the Neumann type were applied on the vertical walls of the enclosure while the horizontal ones are assumed adiabatic. A Carreau–Yasuda model was used to characterize the behavior of the shear thinning fluids. The results revealed the strong influence of the pseudoplastic behavior of a non-Newtonian fluid on its natural convection heat transfer within the enclosure. Results were also obtained by considering the same phenomenon on the basis of the power law model. A comparison was made between the predictions of the two rheological models.

The optimal design of the cited industries is obtained with precision calculation of entropy generation since it clarifies energy losses in a system evidently. Entropy generation on natural convection has been scrutinized in some researches. Ilis et al. [18] investigated entropy generation in rectangular cavities with different aspect ratios numerically. It was demonstrated that heat transfer and fluid friction irreversibility in a cavity vary considerably with the studied aspect ratios. In addition, the total entropy generation in a cavity increases with Rayleigh number, however, the rate of increase depends on the aspect ratio. El-Maghlany et al. [19] analyzed entropy generation associated with laminar natural convection in an infinite square cavity, subjected to an isotropic heat field with various intensities for different Rayleigh numbers. Zu et al. [20] reported a numerical study of entropy generation due to the double-diffusive natural convection in a 3D heterogeneous porous cubic saturated with power-law fluids and submitted to horizontal thermal and concentration gradients.

Lattice Boltzmann method (LBM) has been demonstrated to be a very effective mesoscopic numerical method to model a broad variety of complex fluid flow phenomena [21–26]. The main equations of LBM are hyperbolic and can be solved locally, explicitly, and efficiently on parallel computers. So, the computation process decreases immensely, and the running time drops considerably. However, the specific relation between the relaxation time and the viscosity has caused LBM not to have the considerable success in non-

Newtonian fluid especially on energy equations. In this connection, Fu et al. [27] proposed a new equation for the equilibrium distribution function, modifying the LB model. Here, this equilibrium distribution function is altered in different directions and nodes while the relaxation time is fixed. Independency of the method to the relaxation time in contrast with common LBM provokes the method to solve different non-Newtonian fluid energy equations successfully as the method protects the positive points of LBM simultaneously. In addition, the validation of the method and its mesh independency demonstrates that is more capable than conventional LBM. Huilgol and Kefayati [28] derived the three dimensional equations of continuum mechanics for this method and demonstrated that the theoretical development can be applied to all fluids, whether they be Newtonian, or power law fluids, or viscoelastic and viscoplastic fluids. Following the study, Huilgol and Kefayati [29] developed this method for the Cartesian, cylindrical and spherical coordinates. Recently, Kefayati and Tang [30,31] employed the method to study thermosolutal natural convection and entropy generation of Carreau fluids in a hot enclosure with an inner cold cylinder.
The main aim of this study is to simulate heat and mass transfer, fluid flow, and entropy generation of double diffusive natural convection of a Carreau–Yasuda fluid in a cubic cavity. The innovation of this paper is studying the three dimensional employed code for the Carreau-Yasuda constitutive model. LBM has been employed to study the problem numerically. Moreover, it is endeavored to express the effects of different parameters on entropy generations. The obtained results are validated with previous numerical investigations and the effects of the main parameters are researched.

2 Problem statement

The geometry of the present problem is shown in Fig.1. The temperature and concentration of the left side wall have been considered to be maintained at high temperature and concentration of T_H and C_H as the right side wall is kept at low temperature and concentration of T_C and C_C. The other walls are adiabatic and impermeable. There is no heat generation and thermal radiation. The flow is incompressible, and laminar. The density variation is approximated by the standard Boussinesq model for temperature and concentration as

$$\rho = \rho_0 \left[1 - \beta_T (T - T_0) - \beta_C (C - C_0)\right] , \tag{2.1}$$

where

$$\beta_T = -\frac{1}{\rho_0}\left[\frac{\partial \rho}{\partial T}\right]_C \quad \text{and} \quad \beta_C = -\frac{1}{\rho_0}\left[\frac{\partial \rho}{\partial C}\right]_T , \tag{2.2}$$

where β_T and β_C are thermal and solutal expansion coefficients; respectively. The thermophysical properties of the fluid are taken as constant and they

are estimated at a reference temperature T_0 and solute mass fraction C_0 , which are set to be equal to T_C and C_C , respectively. The cavity is filled with a Carreau–Yasuda fluid. The Prandtl number is fixed at $\mathrm{Pr} = 1$. There is no heat generation, chemical reactions, thermal radiation, Soret, and Dufour parameters. The flow is incompressible, and laminar. The viscous dissipation in the energy equation has been analysed in this study.

3 Dimensional equations

We define the buoyancy velocity scale $U = \left(\frac{\alpha}{L}\right) \mathrm{Ra}^{0.5}$ as Ra is the Rayleigh number. In order to proceed to the numerical solution of the system, the following non dimensional variables are introduced [30,31].

$$t^* = \frac{t\,U}{L}, \quad \mathbf{x}^* = \frac{\mathbf{x}}{L}, \quad \mathbf{u}^* = \frac{\mathbf{u}}{U}, \quad p^* = \frac{p}{\rho\,U^2}, \quad \boldsymbol{\tau}^* = \frac{\boldsymbol{\tau}\,L}{\eta\,U} \tag{3.1}$$

$$T^* = \frac{(T - T_C)}{\Delta T}, \quad \Delta T = T_H - T_C, \quad C^* = \frac{(C - C_C)}{\Delta C}, \quad \Delta C = C_H - C_C \tag{3.2}$$

By substitution of Eqs. (2.3) - (2.4) in dimensional equations and dropping the asterisks, the following system of non-dimensional mass, momentum, energy, and concentration equations are derived.

$$\frac{\partial u}{\partial x} + \frac{\partial v}{\partial y} + \frac{\partial w}{\partial z} = 0 \tag{3.3}$$

$$\frac{\partial u}{\partial t} + u\frac{\partial u}{\partial x} + v\frac{\partial u}{\partial y} + w\frac{\partial u}{\partial z} = -\frac{\partial p}{\partial x} + \frac{\mathrm{Pr}}{\sqrt{\mathrm{Ra}}}\left(\frac{\partial \tau_{xx}}{\partial x} + \frac{\partial \tau_{xy}}{\partial y} + \frac{\partial \tau_{xz}}{\partial z}\right) \tag{3.4}$$

$$\frac{\partial v}{\partial t} + u\frac{\partial v}{\partial x} + v\frac{\partial v}{\partial y} + w\frac{\partial v}{\partial z} = -\frac{\partial p}{\partial y} + \frac{\mathrm{Pr}}{\sqrt{\mathrm{Ra}}}\left(\frac{\partial \tau_{xy}}{\partial x} + \frac{\partial \tau_{yy}}{\partial y} + \frac{\partial \tau_{yz}}{\partial z}\right) \tag{3.5}$$

$$\begin{aligned} \frac{\partial w}{\partial t} + u\frac{\partial w}{\partial x} + v\frac{\partial w}{\partial y} + w\frac{\partial w}{\partial z} &= -\frac{\partial p}{\partial z} \\ + \frac{\mathrm{Pr}}{\sqrt{\mathrm{Ra}}}\left(\frac{\partial \tau_{zx}}{\partial x} + \frac{\partial \tau_{zy}}{\partial y} + \frac{\partial \tau_{zz}}{\partial z}\right) &+ \mathrm{Pr}\,(T + N\,C), \end{aligned} \tag{3.6}$$

$$\frac{\partial T}{\partial t}+u\frac{\partial T}{\partial x}+v\frac{\partial T}{\partial y}+w\frac{\partial T}{\partial z}=\frac{1}{\sqrt{\mathrm{Ra}}}\left(\frac{\partial^2 T}{\partial x^2}+\frac{\partial^2 T}{\partial y^2}+\frac{\partial^2 T}{\partial z^2}\right)$$
$$+\frac{\mathrm{Pr\ Ec}}{\sqrt{\mathrm{Ra}}}\left[\tau_{xx}\left(\frac{\partial u}{\partial x}\right)+\tau_{yy}\left(\frac{\partial v}{\partial y}\right)+\tau_{zz}\left(\frac{\partial w}{\partial z}\right)\right] \tag{3.7}$$
$$+\frac{\mathrm{Pr\ Ec}}{\sqrt{\mathrm{Ra}}}\left[\tau_{xy}\left(\frac{\partial u}{\partial y}+\frac{\partial v}{\partial x}\right)+\tau_{xz}\left(\frac{\partial u}{\partial z}+\frac{\partial w}{\partial x}\right)+\tau_{yz}\left(\frac{\partial v}{\partial z}+\frac{\partial w}{\partial y}\right)\right]$$

$$\frac{\partial C}{\partial t}+u\frac{\partial C}{\partial x}+v\frac{\partial C}{\partial y}+w\frac{\partial C}{\partial z}=\frac{1}{\mathrm{Le}\sqrt{\mathrm{Ra}}}\left(\frac{\partial^2 C}{\partial x^2}+\frac{\partial^2 C}{\partial y^2}+\frac{\partial^2 C}{\partial z^2}\right) \tag{3.8}$$

3.1 Non-dimensional equations of entropy generation

The local dimensionless entropy generations with consideration to non-dimensional variables of Eqs. (2.3) - (2.4) can be acquired as follows [31]

$$S_S=S_F+S_T+S_D \tag{3.9}$$

$$S_F=\Phi_I\left[I+II\right]\ , \tag{3.10}$$

The parameters I and II are obtained from Eqs. (2.13) - (2.14).

$$S_T=\left[\left(\frac{\partial T}{\partial x}\right)^2+\left(\frac{\partial T}{\partial y}\right)^2+\left(\frac{\partial T}{\partial z}\right)^2\right]\ , \tag{3.11}$$

$$S_D=\Phi_{II}\left[\left(\frac{\partial C}{\partial x}\right)^2+\left(\frac{\partial C}{\partial y}\right)^2+\left(\frac{\partial C}{\partial z}\right)^2\right]$$
$$+\Phi_{III}\left[\left(\frac{\partial C}{\partial x}\right)\left(\frac{\partial T}{\partial x}\right)+\left(\frac{\partial C}{\partial y}\right)\left(\frac{\partial T}{\partial y}\right)+\left(\frac{\partial C}{\partial z}\right)\left(\frac{\partial T}{\partial z}\right)\right]\ , \tag{3.12}$$

$$Be=\frac{S_T+S_D}{S_S}\ , \tag{3.13}$$

$$\Phi_I=\frac{\eta(\dot{\gamma})\,T_0}{k}\left(\frac{\alpha}{L\Delta T}\right)^2 Ra\ , \tag{3.14}$$

$$\Omega\ =\frac{T_0}{k}\left(\frac{\alpha}{L\Delta T}\right)^2 \tag{3.15}$$

$$\Phi_{II} = \frac{RDT_0}{kC_0}\left(\frac{\Delta C}{\Delta T}\right)^2 \tag{3.16}$$

$$\Phi_{III} = \frac{RD}{k}\left(\frac{\Delta C}{\Delta T}\right) \tag{3.17}$$

It should be mentioned that the variables of Φ_{II}, Φ_{III}, Ω is taken constant and they are Φ_{II}= 0.5,Φ_{III}= 0.01, Ω = 0.0001.

The local non-dimensional Bejan number is calculated as follows:

$$Be = \frac{S_T + S_D}{S_S}\ , \tag{3.18}$$

The total dimensionless entropy generations are obtained by numerical integration of the local dimensionless entropy generation over the entire cavity volume. It is given by:

$$SF = \int_0^1\int_0^1\int_0^1 S_F\, dxdydz\,, \quad ST = \int_0^1\int_0^1\int_0^1 S_T\, dxdydz, \quad SD = \int_0^1\int_0^1\int_0^1 S_D\, dxdydz, \tag{3.19}$$

$$SS = \int_0^1\int_0^1\int_0^1 S_S\, dxdydz, \quad Be_{avg} = \int_0^1\int_0^1\int_0^1 Be\, dxdydz \tag{3.20}$$

4 Non-dimensional equations

We define the buoyancy velocity scale $U = \left(\frac{\alpha}{L}\right)\mathrm{Ra}^{0.5}$ as Ra is the Rayleigh number. In order to proceed to the numerical solution of the system, the following non dimensional variables are introduced [30,31].

$$t^* = \frac{t\,U}{L}, \quad \mathbf{x}^* = \frac{\mathbf{x}}{L}, \quad \mathbf{u}^* = \frac{\mathbf{u}}{U}, \quad p^* = \frac{p}{\rho\,U^2}, \quad \boldsymbol{\tau}^* = \frac{\boldsymbol{\tau}\,L}{\eta\,U} \tag{4.1}$$

$$T^* = \frac{(T - T_C)}{\Delta T}, \quad \Delta T = T_H - T_C, \quad C^* = \frac{(C - C_C)}{\Delta C}, \quad \Delta C = C_H - C_C \tag{4.2}$$

By substitution of Eqs. (2.3) - (2.4) in dimensional equations and dropping the asterisks, the following system of non-dimensional mass, momentum, energy,

and concentration equations are derived.

$$\frac{\partial u}{\partial x}+\frac{\partial v}{\partial y}+\frac{\partial w}{\partial z}=0 \tag{4.3}$$

$$\frac{\partial u}{\partial t}+u\frac{\partial u}{\partial x}+v\frac{\partial u}{\partial y}+w\frac{\partial u}{\partial z}=-\frac{\partial p}{\partial x}+\frac{\mathrm{Pr}}{\sqrt{\mathrm{Ra}}}\left(\frac{\partial \tau_{xx}}{\partial x}+\frac{\partial \tau_{xy}}{\partial y}+\frac{\partial \tau_{xz}}{\partial z}\right) \tag{4.4}$$

$$\frac{\partial v}{\partial t}+u\frac{\partial v}{\partial x}+v\frac{\partial v}{\partial y}+w\frac{\partial v}{\partial z}=-\frac{\partial p}{\partial y}+\frac{\mathrm{Pr}}{\sqrt{\mathrm{Ra}}}\left(\frac{\partial \tau_{xy}}{\partial x}+\frac{\partial \tau_{yy}}{\partial y}+\frac{\partial \tau_{yz}}{\partial z}\right) \tag{4.5}$$

$$\begin{aligned}\frac{\partial w}{\partial t}+u\frac{\partial w}{\partial x}+v\frac{\partial w}{\partial y}+w\frac{\partial w}{\partial z}&=-\frac{\partial p}{\partial z}\\ +\frac{\mathrm{Pr}}{\sqrt{\mathrm{Ra}}}\left(\frac{\partial \tau_{zx}}{\partial x}+\frac{\partial \tau_{zy}}{\partial y}+\frac{\partial \tau_{zz}}{\partial z}\right)&+\mathrm{Pr}\,(T+N\,C),\end{aligned} \tag{4.6}$$

$$\begin{aligned}\frac{\partial T}{\partial t}+u\frac{\partial T}{\partial x}+v\frac{\partial T}{\partial y}+w\frac{\partial T}{\partial z}&=\frac{1}{\sqrt{\mathrm{Ra}}}\left(\frac{\partial^2 T}{\partial x^2}+\frac{\partial^2 T}{\partial y^2}+\frac{\partial^2 T}{\partial z^2}\right)\\ +\frac{\mathrm{Pr\ Ec}}{\sqrt{\mathrm{Ra}}}&\left[\tau_{xx}\left(\frac{\partial u}{\partial x}\right)+\tau_{yy}\left(\frac{\partial v}{\partial y}\right)+\tau_{zz}\left(\frac{\partial w}{\partial z}\right)\right]\\ +\frac{\mathrm{Pr\ Ec}}{\sqrt{\mathrm{Ra}}}&\left[\tau_{xy}\left(\frac{\partial u}{\partial y}+\frac{\partial v}{\partial x}\right)+\tau_{xz}\left(\frac{\partial u}{\partial z}+\frac{\partial w}{\partial x}\right)+\tau_{yz}\left(\frac{\partial v}{\partial z}+\frac{\partial w}{\partial y}\right)\right]\end{aligned} \tag{4.7}$$

$$\frac{\partial C}{\partial t}+u\frac{\partial C}{\partial x}+v\frac{\partial C}{\partial y}+w\frac{\partial C}{\partial z}=\frac{1}{\mathrm{Le}\sqrt{\mathrm{Ra}}}\left(\frac{\partial^2 C}{\partial x^2}+\frac{\partial^2 C}{\partial y^2}+\frac{\partial^2 C}{\partial z^2}\right) \tag{4.8}$$

The non-dimensional apparent viscosity is given by [30,31]

$$\eta(\dot{\gamma})=\frac{\eta_\infty}{\eta_0}+(1-\frac{\eta_\infty}{\eta_0})\ [1+(Cu\dot{\gamma})^m]^{(n-1)/m}\quad , \tag{4.9}$$

$$\dot{\gamma}=(I+II)^{\frac{1}{2}}\cdot \tag{4.10}$$

$$I=2\left[\left(\frac{\partial u}{\partial x}\right)^2+\left(\frac{\partial v}{\partial y}\right)^2+\left(\frac{\partial w}{\partial z}\right)^2\right] \tag{4.11}$$

$$II = \left(\frac{\partial v}{\partial x} + \frac{\partial u}{\partial y}\right)^2 + \left(\frac{\partial u}{\partial z} + \frac{\partial w}{\partial x}\right)^2 + \left(\frac{\partial v}{\partial z} + \frac{\partial w}{\partial y}\right)^2 \tag{4.12}$$

The ratio η_∞/η_0 has been fixed at 0.0001.

Hence, the stresses are:

$$\tau_{xx} = 2\eta(\dot{\gamma})\left(\frac{\partial u}{\partial x}\right) \quad \tau_{yy} = 2\eta(\dot{\gamma})\left(\frac{\partial v}{\partial y}\right) \quad \tau_{xy} = \eta(\dot{\gamma})\left(\frac{\partial u}{\partial y} + \frac{\partial v}{\partial x}\right) \tag{4.13}$$

The non-dimensional parameters and their physical meanings for the problem are as follows:

Rayleigh number (Ra):

$$\mathrm{Ra} = \frac{\rho\,\beta_T\,gL^3\Delta T}{\eta\,\alpha} \tag{4.14}$$

Prandtl number (Pr):

$$\mathrm{Pr} = \frac{\eta_0}{\rho\,\alpha} \tag{4.15}$$

Eckert number (Ec):

$$\mathrm{Ec} = \frac{U^2}{c_p\,\Delta T} \tag{4.16}$$

Buoyancy ratio number (N):

$$\mathrm{N} = \frac{\Delta C\ \beta_T\ D}{\beta_C\ \Delta T\ \alpha} \tag{4.17}$$

Lewis number (Le):

$$\mathrm{Le} = \frac{\alpha}{D} \tag{4.18}$$

Carreau number (Cu):

$$\mathrm{Cu} = \frac{\lambda\,U}{L} \tag{4.19}$$

Since the buoyancy velocity scale is $U = \left(\frac{\alpha}{L}\right)\mathrm{Ra}^{0.5}$, ΔT and L are equal to unity, the Eckert number has the following relation to the specific heat at

constant pressure, Rayleigh number, and thermal diffusivity

$$\mathrm{Ec} \propto \frac{\alpha^2 \,\mathrm{Ra}}{c_p}\,, \tag{4.20}$$

The α and c_p for different Carreau–Yasuda fluids in various temperatures can be ranged over (10^{-3} – 10^{-6} m^2/s) and (10^2 – 10^4 J/kg K). So, in the highest studied Rayleigh numbers ($\mathrm{Ra} = 10^5$), and the thermal diffusivity ($\alpha = 10^{-3}$) as well as the lowest value of the specific heat at constant pressure, $c_p = 10^2$, the highest amount of the Eckert number would be $\mathrm{Ec} = 0.001$. Therefore, the Eckert number in practical view would be in the range of $\mathrm{Ec} \ll 0.001$. In this study, we have fixed the Eckert number at $\mathrm{Ec} = 0.001$.

The local and the average Nusselt and Sherwood numbers at the hot side wall is as

$$Nu = \left(-\frac{\partial T}{\partial x}\right)_{x=0}, \quad Sh = \left(-\frac{\partial C}{\partial x}\right)_{x=0}, \tag{4.21a}$$

$$Nu_{avg} = \int_0^1 \int_0^1 Nu\, dydz, \quad Sh_{avg} = \int_0^1 \int_0^1 Sh\, dydz \tag{4.21b}$$

4.1 Non-dimensional equations of entropy generation

The local dimensionless entropy generations with consideration to non-dimensional variables of Eqs. (2.3) - (2.4) can be acquired as follows [31]

$$S_S = S_F + S_T + S_D \tag{4.22}$$

$$S_F = \Phi_I \left[I + II\right]\,, \tag{4.23}$$

The parameters I and II are obtained from Eqs. (2.13) - (2.14).

$$S_T = \left[\left(\frac{\partial T}{\partial x}\right)^2 + \left(\frac{\partial T}{\partial y}\right)^2 + \left(\frac{\partial T}{\partial z}\right)^2\right]\,, \tag{4.24}$$

$$\begin{aligned} S_D = \Phi_{II} &\left[\left(\frac{\partial C}{\partial x}\right)^2 + \left(\frac{\partial C}{\partial y}\right)^2 + \left(\frac{\partial C}{\partial z}\right)^2\right] \\ +\Phi_{III} &\left[\left(\frac{\partial C}{\partial x}\right)\left(\frac{\partial T}{\partial x}\right) + \left(\frac{\partial C}{\partial y}\right)\left(\frac{\partial T}{\partial y}\right) + \left(\frac{\partial C}{\partial z}\right)\left(\frac{\partial T}{\partial z}\right)\right]\,, \end{aligned} \tag{4.25}$$

$$Be = \frac{S_T + S_D}{S_S}\,, \tag{4.26}$$

$$\Phi_I = \frac{\eta(\dot{\gamma})\, T_0}{k} \left(\frac{\alpha}{L\Delta T}\right)^2 Ra \ , \tag{4.27}$$

$$\Omega \ = \frac{T_0}{k} \left(\frac{\alpha}{L\Delta T}\right)^2 \tag{4.28}$$

$$\Phi_{II} = \frac{RDT_0}{kC_0} \left(\frac{\Delta C}{\Delta T}\right)^2 \tag{4.29}$$

$$\Phi_{III} = \frac{RD}{k} \left(\frac{\Delta C}{\Delta T}\right) \tag{4.30}$$

It should be mentioned that the variables of Φ_{II}, Φ_{III}, Ω is taken constant and they are Φ_{II}= 0.5,Φ_{III}= 0.01, Ω = 0.0001.

The local non-dimensional Bejan number is calculated as follows:

$$Be = \frac{S_T + S_D}{S_S} \ , \tag{4.31}$$

The total dimensionless entropy generations are obtained by numerical integration of the local dimensionless entropy generation over the entire cavity volume. It is given by:

$$SF = \int_0^1 \int_0^1 \int_0^1 S_F \, dxdydz \, , \quad ST = \int_0^1 \int_0^1 \int_0^1 S_T \, dxdydz, \quad SD = \int_0^1 \int_0^1 \int_0^1 S_D \, dxdydz, \tag{4.32}$$

$$SS = \int_0^1 \int_0^1 \int_0^1 S_S \, dxdydz, \quad Be_{avg} = \int_0^1 \int_0^1 \int_0^1 Be \, dxdydz \tag{4.33}$$

5 The numerical method

The FDLBM equations and their relationships with continuum equations have been explained for two and three dimensional studies in details in Huilgol and Kefayati [28,29]. Here, just a brief description about the main equations would be cited. In addition, the applied algorithm has been described and the studied problem equations in the FDLBM are mentioned.

5.1 The Continuity and Momentum equations

To have the continuity and momentum equations, a discrete particle distribution function f_α is defined over a D3Q15 lattice where it should satisfy an evolution equation:

$$\frac{\partial f_\alpha}{\partial t} + \boldsymbol{\xi}_\alpha \cdot \nabla_{\mathbf{x}} f_\alpha - F_\alpha = -\frac{1}{\varepsilon\ \phi}(f_\alpha - f_\alpha^{eq}), \tag{5.1}$$

where ε is a small parameter to be prescribed when numerical simulations are considered. ϕ is the relaxation time and F_α is the external force.

Associated to each node is a lattice velocity vector $\boldsymbol{\xi}_\alpha$. It is defined as follows:

Node	Location	$\boldsymbol{\xi}_\alpha/\sigma$
α_0	(0, 0, 0)	$\mathbf{0}$
α_1	(1, 0, 0)	$\mathbf{i}$
α_2	(0, 1, 0)	$\mathbf{j}$
α_3	(-1, 0, 0)	$-\mathbf{i}$
α_4	(0, -1, 0)	$-\mathbf{j}$
α_5	(0, 0, 1)	$\mathbf{k}$
α_6	(0, 0, -1)	$-\mathbf{k}$
α_7	(1, 1, 1)	$\mathbf{i}+\mathbf{j}+\mathbf{k}$
α_8	(-1, 1, 1)	$-\mathbf{i}+\mathbf{j}+\mathbf{k}$
α_9	(-1, -1, 1)	$-\mathbf{i}-\mathbf{j}+\mathbf{k}$
α_{10}	(1, -1, 1)	$\mathbf{i}-\mathbf{j}+\mathbf{k}$
α_{11}	(1, 1, -1)	$\mathbf{i}+\mathbf{j}-\mathbf{k}$
α_{12}	(-1 , 1, -1)	$-\mathbf{i}+\mathbf{j}-\mathbf{k}$
α_{13}	(-1, -1, -1)	$-\mathbf{i}-\mathbf{j}-\mathbf{k}$
α_{14}	(1, -1, -1)	$\mathbf{i}-\mathbf{j}-\mathbf{k}$

The constant σ has to be chosen with care for it affects numerical stability; its choice depends on the problem. The method for finding the parameter σ which satisfies the Courant-Friedrichs-Lewy (CFL) condition is described in [28,29].

The equilibrium distribution function, f_α^{eq}, is different from the conventional

ones adopted by previous researchers, who normally expand the Maxwellian distribution function. In the present approach, we expand f_α^{eq} as a quadratic in terms of $\boldsymbol{\xi}_\alpha$, using the notation of linear algebra [28,29]:

$$f_\alpha^{eq} = A_\alpha + \boldsymbol{\xi}_\alpha \cdot \mathbf{B}_\alpha + (\boldsymbol{\xi}_\alpha \otimes \boldsymbol{\xi}_\alpha) : \mathbf{C}_\alpha, \ \alpha = 0, 1, 2, \cdots, 14. \tag{5.2}$$

Here, the scalars A_α are defined through

$$A_0 = \rho - \frac{2p}{\sigma^2} - \frac{\rho|\mathbf{u}|^2}{\sigma^2} + \frac{\tau_{xx} + \tau_{yy} + \tau_{zz}}{\sigma^2}, \quad A_\alpha = 0, \ \alpha = 1, 2, \cdots, 14. \tag{5.3}$$

The vectors $\mathbf{B}_\alpha$ are given by

$$\mathbf{B}_\alpha = \frac{\rho \mathbf{u}}{2\sigma^2}, \ \alpha = 1, .., 6; \quad \mathbf{B}_\alpha = \mathbf{0}, \ \alpha = 0, 7, .., 14. \tag{5.4}$$

Next, the matrices $\mathbf{C}_\alpha$ are such that $\mathbf{C}_0 = 0$; $\mathbf{C}_1 = \mathbf{C}_\alpha$, $\alpha = 1, ..., 6$; $\mathbf{C}_2 = \mathbf{C}_\alpha$, $\alpha = 0, 7, ..., 14$ where

$$\begin{gathered} \mathbf{C}_1 = \begin{bmatrix} C_{11} & 0 & 0 \\ 0 & C_{22} & 0 \\ 0 & 0 & C_{33} \end{bmatrix}, \quad C_{11} = \frac{1}{2\sigma^4}(p + \rho u^2 - \frac{\mathrm{Pr}}{\sqrt{\mathrm{Ra}}}\tau_{xx}), \quad , \\ C_{22} = \frac{1}{2\sigma^4}(p + \rho v^2 - \frac{\mathrm{Pr}}{\sqrt{\mathrm{Ra}}}\tau_{yy}) \quad C_{33} = \frac{1}{2\sigma^4}(p + \rho w^2 - \frac{\mathrm{Pr}}{\sqrt{\mathrm{Ra}}}\tau_{zz}) \end{gathered} \tag{5.5}$$

$$\begin{gathered} \mathbf{C}_2 = \begin{bmatrix} 0 & C_{12} & C_{13} \\ C_{21} & 0 & C_{23} \\ C_{31} & C_{32} & 0 \end{bmatrix} \quad , C_{12} = C_{21} = \frac{1}{2\sigma^4}(\rho uv - \frac{\mathrm{Pr}}{\sqrt{\mathrm{Ra}}}\tau_{xy}) \\ C_{23} = C_{32} = \frac{1}{2\sigma^2}(\rho vw - \frac{\mathrm{Pr}}{\sqrt{\mathrm{Ra}}}\tau_{yz}) \quad C_{13} = C_{31} = \frac{1}{2\sigma^2}(\rho uw - \frac{\mathrm{Pr}}{\sqrt{\mathrm{Ra}}}\tau_{xz}) \end{gathered} \tag{5.6}$$

The functions F_α is defined as

$$F_\alpha = 0, \quad \alpha = 1, ..., 6 \tag{5.7a}$$

$$F_\alpha = \frac{1}{2\sigma^2}\mathbf{b} \cdot \boldsymbol{\xi}_\alpha, \quad \alpha = 0, 7, ..., 14 \tag{5.7b}$$

$$\mathbf{b} = \mathrm{Pr}\,(T + \mathrm{N}\,C)\mathbf{j} \tag{5.8}$$

5.2 The Energy Equation

In order to obtain the energy equation, an internal energy distribution function g_α is introduced and it is assumed to satisfy an evolution equation similar to that for f_α. Thus,

$$\frac{\partial g_\alpha}{\partial t} + \boldsymbol{\xi}_\alpha \cdot \nabla_{\mathbf{x}} g_\alpha - G_\alpha = -\frac{1}{\varepsilon\phi}(g_\alpha - g_\alpha^{eq}). \tag{5.9}$$

G_α refers to the external supply e.g. radiation in the energy equation. Here, g_α^{eq} has a monomial expansion:

$$g_\alpha^{eq} = D_\alpha + \boldsymbol{\xi}_\alpha \cdot \mathbf{E}_\alpha, \tag{5.10}$$

One way of satisfying the above is to assume, as before, that the scalars are given by $D_\alpha = D_1,\ \alpha = 1, ..., 6$ and $D_\alpha = D_2,\ \alpha = 7, ..., 14$. In this problem, the non-dimensional parameters are obtained as follows:

$$D_0 = T, \quad D_1 = D_2 = 0. \tag{5.11}$$

where

$$\mathbf{E}_\alpha = 0, \quad \alpha = 0, 7, .., 14 \tag{5.12a}$$

$$\mathbf{E}_\alpha = \frac{\left(\mathbf{u}\,T - \frac{\mathrm{Pr\,Ec}}{\sqrt{\mathrm{Ra}}}\ (\mathbf{u}\,\boldsymbol{\tau}) - \frac{1}{\sqrt{\mathrm{Ra}}}\left(\frac{\partial T}{\partial \mathbf{x}}\right)\right)}{2\,\sigma^2}, \quad \alpha = 1, ..., 6 \tag{5.12b}$$

The parameter G_α can be defined as

$$G_\alpha = 0, \quad \alpha = 0, ..., 14 \tag{5.13}$$

5.3 The Concentration Equation

In order to obtain the concentration equation, an internal concentration distribution function h_α is introduced and it is assumed to satisfy an evolution equation similar to that for f_α. Thus,

$$\frac{\partial h_\alpha}{\partial t} + \boldsymbol{\xi}_\alpha \cdot \nabla_{\mathbf{x}} h_\alpha - H_\alpha = -\frac{1}{\varepsilon\phi}(h_\alpha - h_\alpha^{eq}). \tag{5.14}$$

Here, h_α^{eq} has a monomial expansion:

$$h_\alpha^{eq} = M_\alpha + \boldsymbol{\xi}_\alpha \cdot \mathbf{Z}_\alpha, \tag{5.15}$$

One way of satisfying the above is to assume, as before, that the scalars are given by $M_\alpha = M_1,\ \alpha = 1, ..., 6$ and $M_\alpha = M_2,\ \alpha = 0, 7, ..., 14$. In this problem, the non-dimensional parameters are obtained as follows:

$$M_0 = C, \quad M_1 = M_2 = 0. \tag{5.16}$$

where

$$\mathbf{Z}_\alpha = 0, \quad \alpha = 0, 7, ..., 14 \tag{5.17a}$$

$$\mathbf{Z}_\alpha = \frac{\left(\mathbf{u}\, C - \frac{1}{\mathrm{Le}\sqrt{\mathrm{Ra}}}\left(\frac{\partial C}{\partial \mathbf{x}}\right)\right)}{2\,\sigma^2}, \quad \alpha = 1, ..., 6 \tag{5.17b}$$

Finally, $H_\alpha = 0$.

6 Code validation and grid independence

Lattice Boltzmann Method (LBM) scheme is utilized to simulate entropy generation of laminar double diffusive natural convection in a cubic cavity that is filled with a Carreau–Yasuda fluid. The Prandtl, Carreau, and Eckert numbers are fixed at Pr = 1, Cu = 1, and Ec = 0.001; respectively. This problem is investigated at different parameters of Rayleigh number (Ra = 10^4 and 10^5), Power-law index (n = 0.5, 1, and 1.5), the Buoyancy ratio (N = -1, 0.1, and 1), and the Lewis number (Le = 0.5, 2.5, and 10). An extensive mesh testing procedure was conducted to guarantee a grid independent solution. Different mesh combinations were explored for the case of Ra= 10^5, N = 0.1, n = 1.5, and Le = 2.5. The average Nusselt and Sherwood numbers on the hot wall for different meshes have been studied. It was confirmed that the grid size (40*40*40) observing less than 1% difference between results obtained on smaller grids in ensures a grid independent solution as portrayed by Table.1. The running time for the grid size is 48512 seconds. To validate the three dimensional double diffusive natural convection for the case of Newtonian fluid, the average Nusselt and Sherwood numbers on the hot side wall are validated between present results and Sezai and Mohamad [6], and Kuznetsov et al. [8] in the Table.2 in different Rayleigh numbers. The accuracy of the study for Carreau fluids and entropy generation can be observed in the previous studies by the applied code [30,31].

7 Results and discussion

7.1 Effect of Rayleigh number

Fig.2 shows the isotherms, streamlines and isoconcentrations in different Rayleigh numbers at Le = 2.5, N = 0.1, $Cu = m = 1$, and n = 1.5. As the Rayleigh number increases, the movements of the isotherms between the cold and hot side walls ameliorate significantly and they become progressively curved. Moreover, the gradient of temperature on the hot wall augments with the rise of Rayleigh number. In fact, it occurs while the thermal boundary layer thickness on the side walls decreases with increasing Rayleigh number. The streamlines exhibit that the convection process has been enhanced by the growth of Rayleigh numbers as the core of the streamline changes and the streamlines traverse more distance in the cavity. The isoconcentration demonstrates a similar manner where the increase in Rayleigh number rises the gradient of isoconcentrations on the hot walls. It depicts that mass transfer enhances significantly with the rise of Rayleigh number. Table.3 confirms that the average Nusselt and Sherwood numbers enhance as Rayleigh number rises in different power-law indexes. It is observed that the effect of Rayleigh number drops when the power-law index increases.
Fig.3 displays the Rayleigh number effects on entropy generations due to heat transfer (S_T), fluid friction (S_F), mass transfer (S_D), and summation entropy generation (S_S) at Le = 2.5, N = 0.1, $Cu = m = 1$, and n = 1.5. It demonstrates that S_T increases generally, but this augmentation is not uniform in the cavity and in some places we face a decrease in the S_T. The S_F demonstrates that the high values are observed on the sidewalls. Generally, the S_F increases considerably with the rise of Rayleigh number where the minimum value in the center of the cube cavity due to the increase in Rayleigh number. The entropy generation due to mass transfer (S_D) enhances generally with the rise of Rayleigh number; although, this augmentation is less than S_F. It shows the gradient of S_D on the side wall enhances with the rise of Rayleigh number. Interestingly, the increase in Rayleigh number causes a low value section of S_D is generated on the top section of the enclosure which proves that the rise of Rayleigh number decreases the irreversibility due to mass transfer. Table.4 demonstrates that different entropy generations and total entropy generations enhance as Rayleigh number increases in various power-law indexes.

7.2 Effect of power-law index index

Fig.4 shows the isotherms, isoconcentrations and streamlines for different power-law indexes at N = 0.1, Ra = 10^4, $Cu = m = 1$, Le = 2.5. As the

power-law index increases, the movements of the isotherms between the cold and hot side walls declines significantly. Moreover, the gradient of temperature on the hot wall augments with the drop of power-law index. In fact, it occurs while the thermal boundary layer thickness on the side walls decreases with the drop of the power-law index. The streamlines exhibit that the convection process has been enhanced by the decrease of power-law index. The isoconcentration shows that the increase in power-law index declines the isoconcentration movement between the hot and the cold side walls. It depicts that mass transfer drops substantially with the rise of power-law index. Table.3 shows that the increase in power-law index in various Rayleigh numbers decreases the average Nusselt and Sherwood numbers.
Fig.5 indicates the horizontal velocity and temperature in the middle of the cavity, the local Nusselt and sherwood numbers on the left side wall have been studied for different power-law indexes at N = 0.1, Ra = 10^4, $Cu = m = 1$, Le = 2.5. Generally, it displays that the horizontal velocity for different power-law indexes has the maximum values close to the horizontal walls while the minimum magnitudes are observed in the middle of the side wall. The amplitudes of the horizontal velocity magnitude on the top and bottom sides of the cavity do indeed drop with augmentation of power-law index regularly. The local temperature has a curved manner where the minimum values are observed in the middle of the cavity and the values decline marginally as power-law index enhances. The local Nusselt and sherwood numbers on the hot wall drop as the power-law index rises. They demonstrate that the maximum Nusselt and Sherwood numbers appear at Y = 0.2. Further, the increase in power-law index decreases the local Nusselt and sherwood numbers at $Z < 0.5$ while they do not change significantly due to the rise of the power-law index at $Z > 0.5$.
Fig.6 depicts the power-law index effects on entropy generations due to heat transfer (S_T), fluid friction (S_F), mass transfer (S_D), and summation entropy generation (S_S) at N = 0.1, Ra = 10^4, $Cu = m = 1$, Le = 2.5. It shows that the S_T becomes weak slightly as the power-law index increases. It is clear the maximum values of the irreversibility due to heat transfer, mass transfer, fluid friction are close to the side walls since the gradient temperature and velocity in the sections are more significant than other parts of the cavity. In addition, it shows that the shape and value of the local entropy alters with the changes of power-law indexes. In addition, the rise of power-law index declines the entropy generation due to heat transfer and fluid friction. The entropy generation due to mass transfer follows the trend of local entropy generation of heat transfer and fluid friction where the increase in power-law index fall the maximum value. Inevitably, total entropy generation demonstrates a different manner in the middle of the side wall with the rise of the power-law index. Table.4 demonstrates that different entropy generations and total entropy generations decline as power-law index increases in various Rayleigh numbers. It indicates that the rise of power-law index increases and decreases the average Bejan number at Ra = 10^4 and Ra = 10^5, respectively.

7.3 Effect of Buoyancy ratio

Fig.7 depicts the isotherms, streamlines and the isoconcentrations for different buoyancy ratios at Ra = 10^5, n = 1.5, $Cu = m = 1$, Le = 2.5. The comparison between the isotherms demonstrates the rise of the buoyancy ratio from N=-1 to 1 causes the gradient of the isotherms on the hot wall to increase significantly. Hence, the pattern clarifies that the augmentation of buoyancy ratio enhances heat transfer. Moreover, the trend is observed in isoconcentrations as they incline to the hot wall and their gradient augments noticeably. As a result, mass transfer similar to heat transfer is improved by the increase in buoyancy ratio. The shapes of the streamlines in different buoyancy ratios can prove the cited result in the isotherms and isoconcentrations properly. At N=-1, a secondary vortex close to the cold wall weakens the main vortex as it circulates in the opposite direction of the main vortex counterclockwise. In addition, it is evident that the main circulation in the cavity move toward the hot wall as buoyancy ratio enhances from N=0.1 to 1 and, moreover, the separated vortexes in the core of the cavity becomes uniform with an apparent inclination to the hot wall. Table.5 shows that the rise of the buoyancy ratio from N = -1 to 1 increases the average Nusselt and Sherwood numbers in different Rayleigh numbers.
Fig.8 shows the Buoyancy ratio effects on entropy generations due to heat transfer (S_T), fluid friction (S_F), mass transfer (S_D), and summation entropy generation (S_S) at Ra = 10^5, n = 1.5, $Cu = m = 1$, Le = 2.5. It shows that the shape and value of the local entropy generations alter with the changes of buoyancy ratios. In fact, the increase in buoyancy ratios augments the entropy generation markedly and causes the higher values move closer to the sidewalls. Table.6 depicts that the rise of the buoyancy ratio from N = -1 to 1 enhances the irreversibilities due to heat transfer, fluid friction and mass transfer considerably. In addition, the total entropy generation rockets up as the buoyancy ratio augments while the average Bejan number decreases gradually.

7.4 Effect of Lewis number

Fig.9 depicts the isotherms, streamlines and the isoconcentrations for different Lewis numbers at Ra = 10^5, n = 1.5, $Cu = m = 1$, N = 0.1. The contours exhibit that the density of the isoconcentrations on the hot side wall grows significantly with the increase in Lewis numbers. The pattern confirms that mass transfer enhances with the rise of Lewis number considerably. But, the Lewis number does not affect the isotherms and streamlines significantly. Table.7 shows that the average Sherwood numbers increase considerably with the enhancement of Lewis number, but the average Nusselt number changes slightly.

Fig.10 shows the Lewis number effects on entropy generations due to heat transfer (S_T), fluid friction (S_F), mass transfer (S_D), and summation entropy generation (S_S) at Ra = 10^5, n = 1.5, $Cu = m = 1$, N = 0.1. The contours of the local entropy generation and maximum values of the entropy generations demonstrate that the augmentation of Lewis number declines the irreversibilities due to heat transfer and fluid frictions while entropy generation because of mass transfer is strengthen. Table 8 illustrates the average entropy generation due to mass transfer increases with the enhancement of Lewis number for different studied parameters. Further, the total entropy generations due to heat transfer and fluid friction decreases with the growth of Lewis number. The assumption of total entropy generations augment with increase in Lewis number. On the other hand, the average Bejan number increases marginally when Lewis number increases from Le = 2.5 to 10.

7.5 Effect of Carreau–Yasuda model parameter

Table 9 shows that the average Nusselt and Sherwood numbers increase gradually with the enhancement of the Carreau–Yasuda model parameter in different Rayleigh numbers.
Table 10 illustrates various entropy generations rises with the enhancement of the Carreau–Yasuda model parameter for different studied parameters. So, the assumption of total entropy generations augment with increase in the Carreau–Yasuda model parameter. On the other hand, the average Bejan number drops and increases marginally at Ra = 10^4 and 10^5; respectively when the Carreau–Yasuda model parameter increases

7.6 Effect of Carreau number

Fig.11 depicts the isotherms, streamlines and the isoconcentrations for different Carreau numbers at Ra = 10^5, n = 1.5, $m = 1$, Le = 2.5, N = 0.1. The contours demonstrate that the densities of the isotherms and isoconcentrations on the hot side wall drops significantly with the increase in Carreau number. The pattern confirms that heat and mass transfer decline with the rise of Carreau number considerably. In addition, the streamlines prove the trend where the broken vortexes in the middle of the streamlines alters to a uniform vortex. Table.11 shows that the average Sherwood numbers decrease considerably with the enhancement of Carreau number.
Fig.12 shows the Carreau number effects on entropy generations due to heat transfer (S_T), fluid friction (S_F), mass transfer (S_D), and summation entropy generation (S_S) at Ra = 10^5, n = 1.5, $m = 1$, Le = 2.5, N = 0.1. The contours of the local entropy generation and maximum values of the entropy genera-

tions demonstrate that the augmentation of Carreau number declines different irreversibilities. Table 12 indicates different total entropy generations decrease gradually as the Carreau number increases. The assumption of total entropy generations drop with increase in Carreau number. On the other hand, the average Bejan number decreases marginally when Carreau number increases.

8 Concluding Remarks

Thermosolutal natural convection and entropy generation of Carreau–Yasuda fluid in a cubic cavity has been analyzed by Lattice Boltzmann method. This study has been conducted for the pertinent parameters in the following ranges: Rayleigh number (Ra = 10^4 and 10^5), the Buoyancy ratio (N = -1, 0.1, 1), the Lewis number (Le = 0.5, 2.5, 10), power-law indexes (n = 0.5, 1, and 1.5), Carreau number (Cu = 0.01, 0.1, 1, 10 and 100), and Carreau-Yasuda parameter (m = 1, 10, and 100). The main conclusions of the present investigation can be summarized as follows:

- Heat and mass transfer enhance as Rayleigh number augments in different studied parameters.
- The average Nusselt and Sherwood numbers demonstrate that the heat and mass transfer decline since the power-law index rises in various studied parameters.
- The enhancement of the buoyancy ratio increases heat and mass transfer considerably.
- The increase in Lewis number enhances mass transfer and has a minor effect on heat transfer.
- The increase in the Carreau–Yasuda model parameter enhances heat and mass transfer slightly.
- The rise of Carreau number decreases heat and mass transfer significantly.
- The enhancement of Rayleigh number augments different irreversibilities and the highest level of growth is observed at the entropy generation due to fluid friction.
- Bejan number declines significantly with the augmentation of Rayleigh number which demonstrates a jump in the irreversibility due to fluid friction.
- The enhancement of power-law index decreases different entropy generations steadily while the average Bejan number changes marginally.
- The increase in the buoyancy ratio enhances the entropy generations and causes the average Bejan number to drop.
- The rise of Lewis number enhances the entropy generation due to mass transfer for different studied parameters. However, it influences the irreversibilities due to heat transfer and fluid friction marginally.
- The increase in the Carreau–Yasuda model parameter enhances irreversibilities in the system.

- The augmentation of Carreau number decreases irreversibilities considerably.

Acknowledgements

The first author(Gholamreza Kefayati (GH. R. Kefayati)) gratefully acknowledges the funding support in the form of a Research Fellowship awarded him by the Hong Kong Polytechnic University.

References

[1] C. Beghein, F. Haghighat, F. Allard, Numerical study of double-diffusive natural convection in a square cavity, International Journal of Heat and Mass Transfer 35 (1992) 833–846.

[2] R. Bennacer, D. Gobin, Cooperating thermosolutal convection in enclosures I. Scale analysis and mass transfer, International Journal of Heat and Mass Transfer 39 (1996) 2671–2681.

[3] R. Bennacer, D. Gobin, Cooperating thermosolutal convection in enclosures II. Heat transfer and flow structure, International Journal of Heat and Mass Transfer 39 (1996) 2683–2697.

[4] S.H. Xin, P.L. Qur, L.S. Tuckerman, Bifurcation analysis of double-diffusive convection with opposing horizontal thermal and solutal gradients, Phys. Fluids 10 (1998) 850–858.

[5] I. Sezai, Three-dimensional double-diffusive convection in a porous cubic enclosure due to opposing gradients of temperature and concentration, J. Fluid Mech. 400 (1999) 333–353.

[6] I. Sezai, A. A. Mohamad, Double diffusive convection in a cubic enclosure with opposing temperature and concentration gradients, Phys. Fluids 12 (2000) 2210–2223.

[7] I. Sezai, Flow transitions in three-dimensional double-diffusive fingering convection in a porous cavity, J. Fluid Mech. 464 (2002) 311–344.

[8] Geniy V. Kuznetsov, Mikhail A. Sheremet, A numerical simulation of double-diffusive conjugate natural convection in an enclosure, International Journal of Thermal Sciences 50 (2011) 1878–1886.

[9] GH. R. Kefayati, FDLBM simulation of entropy generation in double diffusive natural convection of power-law fluids in an enclosure with Soret and Dufour effects, International Journal of Heat and Mass Transfer 89 (2015) 267–290.

[10] Q. Y. Zhu, Y. J. Zhuang, H. Z. Yu, Three-dimensional numerical investigation on thermosolutal convection of power-law fluids in anisotropic porous media, International Journal of Heat and Mass Transfer 104 (2017) 897–917.

[11] P. J. Carreau, Rheological equations from molecular network theories, Trans Soc Rheol 16 (1972) 99-127.

[12] K. Yasuda, Investigation of the analogies between viscometric and linear viscoelastic properties of polystyrene fluids, PhD Thesis (1979) Massachusetts Institute Technology, Department of Chemical Engineering.

[13] A. Shamekhi, K. Sadeghy, Cavity flow simulation of Carreau–Yasuda non-Newtonian fluids using PIM meshfree method, Applied Mathematical Modelling 33 (2009) 4131-4145.

[14] M. Bouteraa, C. Nouar1, E. Plaut, C. Metivier, A. Kalck, Weakly nonlinear analysis of Rayleigh Benard convection in shear-thinning fluids: nature of the bifurcation and pattern selection, J. Fluid Mech. 767 (2015) 696-734.

[15] A. Pantokratoras, Steady flow of a non-Newtonian Carreau fluid across an unconfined circular cylinder, Meccanica 51 (2016) 1007-1016.

[16] S. Shahsavari, G. H. McKinley, Mobility of Power-law and Carreau Fluids through Fibrous Media, Physical review E, Statistical, nonlinear, and soft matter physics 92 (2015) pp.063012.

[17] Z. Alloui, P. Vasseur, Natural convection of Carreau–Yasuda non-Newtonian fluids in a vertical cavity heated from the sides, International Journal of Heat and Mass Transfer 84 (2015) 912–924.

[18] G.G. Ilis, M. Mobedi, B. Sunden, Effect of aspect ratio on entropy generation in a rectangular cavity with differentially heated vertical walls, International Communications in Heat and Mass Transfer 35 (2008) 696-703.

[19] W. M. El-Maghlany, K.M. Saqr, M. A. Teamah, Numerical simulations of the effect of an isotropic heat field on the entropy generation due to natural convection in a square cavity, Energy Conversion and Management 85 (2014) 333-342.

[20] Q.Y. Zhu, Y.J. Zhuang, H.Z. Yu, Entropy generation due to three-dimensional double-diffusive convection of power-law fluids in heterogeneous porous media, International Journal of Heat and Mass Transfer 106 (2017) 61–82.

[21] A. A. Mehrizi, M. Farhadi, S. Shayamehr, Natural convection flow of Cu-Water nanofluid in horizontal cylindrical annuli with inner triangular cylinder using lattice Boltzmann method, International Communications in Heat and Mass Transfer 44 (2013) 147-156.

[22] A. A. Mehrizi, M. Farhadi, K. Sedighi, M. A. Delavar, Effect of fin position and porosity on heat transfer improvement in a plate porous media heat exchanger, Journal of the Taiwan Institute of Chemical Engineers 44 (2013) 420-431.

[23] H. R. Ashorynejad, B. Hoseinpour, Investigation of different nanofluids effect on entropy generation on natural convection in a porous cavity, European Journal of Mechanics B/Fluids 62 (2017) 86-93.

[24] H. Sajjadi, M. Salmanzadeh, G. Ahmadi, S. Jafari, Turbulent indoor airflow simulation using hybrid LES/RANS model utilizing Lattice Boltzmann method, Computers and Fluids 150 (2017) 66-73.

[25] H. R. Ashorynejad, K. Javaherdeh, Investigation of a waveform cathode channel on the performance of a PEM fuel cell by means of a pore-scale multi-component lattice Boltzmann method, Journal of the Taiwan Institute of Chemical Engineers, 66 (2016) 126-136.

[26] H. Sajjadi, M. Salmanzadeh, G. Ahmadi, S. Jafari, Simulations of indoor airflow and particle dispersion and deposition by the lattice Boltzmann method using LES and RANS approaches, Building and Environment 102 (2016) 1-12.

[27] S.C. Fu, R.M.C. So, W.W.F. Leung, Linearized-Boltzmann-type-equation-based finite difference method for thermal incompressible flow, Computers and Fluids 69 (2012) 67-80.

[28] R. R. Huilgol, GH. R. Kefayati, From mesoscopic models to continuum mechanics: Newtonian and non-Newtonian fluids, Journal of Non-Newtonian Fluid Mechanics 233 (2016) 146-154.

[29] R. R. Huilgol, GH. R. Kefayati, A particle distribution function approach to the equations of continuum mechanics in Cartesian, cylindrical and spherical coordinates: Newtonian and non-Newtonian Fluids, Journal of Non-Newtonian Fluid Mechanics 251 (2018) 119–131.

[30] GH.R. Kefayati, H. Tang, Double-diffusive natural convection and entropy generation of Carreau fluid in a heated enclosure with an inner circular cold cylinder (Part I: Heat and mass transfer), International Journal of Heat and Mass Transfer 120 (2018) 731–750.

[31] GH.R. Kefayati, H. Tang, Double-diffusive natural convection and entropy generation of Carreau fluid in a heated enclosure with an inner circular cold cylinder (Part II: Entropy generation), International Journal of Heat and Mass Transfer 120 (2018) 683–713.

Nomenclature

Be Bejan number
$\mathbf{b}$ Body force
C Concentration
c Lattice speed
c_p Specific heat capacity at constant pressure
Cu Carreau number
D Mass diffusivity
$\mathbf{D}$ Deformation rate tensor
Ec Eckert number
F External forces
f_α Density distribution functions for the specific node of α
f_α^{eq} Equilibrium density distribution functions for the specific node of α
g_α Internal energy distribution functions for the specific node of α
g_α^{eq} Equilibrium internal energy distribution functions for the specific node of α
g Gravity
h_α Internal concentration distribution functions for the specific node of α
h_α^{eq} Equilibrium internal concentration distribution functions for the specific node of α
k Thermal conductivity
L Length of the cavity
Le Lewis number
m Carreau-Yasuda model parameter
n Power-law index
N Buoyancy ratio
Nu Nusselt number
p Pressure
Pr Prandtl number
R Gas constant
Ra Rayleigh number
Sh Sherwood number
S_D Local entropy generation due to mass transfer
S_F Local entropy generation due to fluid friction
S_S Local summation entropy generation
S_T Local entropy generation due to heat transfer
SD Total entropy generation due to mass transfer
SF Total entropy generation due to fluid friction
SS Total summation entropy generation
ST Total entropy generation due to heat transfer
T Temperature
t Time
x, y, z Cartesian coordinates

u Velocity in x direction
v Velocity in y direction
w Velocity in z direction

Greek letters

β_T Thermal expansion coefficient
β_C Solutal expansion coefficient
ϕ Relaxation time
τ Shear stress
ξ Discrete particle speeds
Δx Lattice spacing
Δt Time increment
α Thermal diffusivity
ρ Density of fluid
η Dynamic viscosity
η_0 Zero shear viscosity
η_∞ Infinite shear viscosity
ψ Stream function value
λ Time constant
$\dot{\gamma}$ Shear rate

Subscripts

avg Average
B Bottom
C Cold
H Hot
L Left
x, y, z Cartesian coordinates
α Specific node
T Thermal
D Solutal

Table 1
Grid independence study at Ra = 10^5, n = 1.5, Le = 2.5, $m = 1, Cu = 1$ and N = 0.1

Mesh size	Nu_{avg}	Sh_{avg}
30*30*30	3.9208	6.5751
40*40*40	3.5954	6.0307
50*50*50	3.5941	6.0301
60*60*60	3.5932	6.0292

Table 2
Variations of the average Nusselt and Sherwood numbers with Rayleigh number for Pr = Le = 10, $m = 1, Cu = 1$, N = -0.5

	Present study	Sezai and Mohamad [6]	Kuznetsov et al. [8]
Ra = 10^3			
Nu_{avg}	1	1.0	1.06
Sh_{avg}	2.44	2.5	2.39
Ra = 10^4			
Nu_{avg}	2.03	2.0	2.01
Sh_{avg}	5.08	4.92	5.18
Ra = 10^5			
Nu_{avg}	3.88	3.82	–
Sh_{avg}	6.61	6.52	–

Table 3
The average Nusselt and Sherwood numbers in various Rayleigh numbers, and power-law indexes at N = 0.1 $m = 1, Cu = 1$ and Le = 2.5

Ra = 10^4	n = 0.5	n = 1	n = 1.5
Nu_{avg}	2.298	1.978	1.811
Sh_{avg}	3.866	3.430	3.210
Ra = 10^5			
Nu_{avg}	5.225	4.041	3.595
Sh_{avg}	8.706	6.675	6.031

Table 4
Different entropy generations and average Bejan numbers in various power-law indexes at Ra = 10^4 $m = 1, Cu = 1$ and N = 0.1

	ST	SF	SD	SS	Be_{avg}
Ra = 10^4					
n=0.5	3.172	1.804	2.621	7.534	0.755
n=1	2.574	1.326	2.081	5.917	0.766
n=1.5	2.278	1.108	1.854	5.176	0.777
Ra = 10^5					
n=0.5	8.275	41.720	7.869	57.804	0.410
n=1	5.674	30.958	4.737	41.307	0.375
n=1.5	4.732	24.252	3.836	32.759	0.371

Table 5
Effects of the Buoyancy ratio (N) on the average Nusselt and Sherwood numbers in different Rayleigh numbers at n = 1.5, $m = 1, Cu = 1$ and Le = 2.5

	N = 0.1	N = 1	N = -1
Ra = 10^4			
Nu_{avg}	1.811	2.096	1.440
Sh_{avg}	3.210	3.973	2.231
Ra = 10^5			
Nu_{avg}	3.595	3.819	1.758
Sh_{avg}	6.031	6.671	2.617

Table 6
Effects of the Buoyancy ratio (N) on different entropy generations and average Bejan number in different Rayleigh numbers at n = 1.5, $m = 1, Cu = 1$ and Le = 2.5

	N = 0.1	N = 1	N = -1
Ra = 10^4			
ST	2.278	2.513	1.489
SF	1.108	1.933	0.196
SD	1.854	2.264	1.038
SS	5.176	6.646	2.658
Be_{avg}	0.777	0.727	0.921
Ra = 10^5			
ST	4.732	5.252	2.355
SF	24.252	42.391	5.635
SD	3.836	4.413	1.657
SS	32.759	51.996	9.581
Be_{avg}	0.371	0.373	0.401

Table 7
Effects of the Lewis number (Le) on the average Nusselt and Sherwood numbers in different Rayleigh numbers at n = 1.5, $m = 1, Cu = 1$ and N = 0.1

	Le = 0.5	Le = 2.5	Le = 10
Ra = 10^4			
Nu_{avg}	2.004	1.811	1.966
Sh_{avg}	1.335	3.210	6.645
Ra = 10^5			
Nu_{avg}	3.632	3.595	3.561
Sh_{avg}	2.344	6.031	11.329

Table 8
Effects of the Lewis number (Le) on different entropy generations and average Bejan number in different Rayleigh numbers at n = 1.5, $m = 1, Cu = 1$ and N = 0.1

	Le = 0.5	Le = 2.5	Le = 10
Ra = 10^4			
ST	2.355	2.278	2.288
SF	1.195	1.108	1.060
SD	0.865	1.854	4.167
SS	4.351	5.176	7.452
Be_{avg}	0.750	0.777	0.799
Ra = 10^5			
ST	4.732	4.813	4.676
SF	24.252	26.260	23.249
SD	3.836	1.622	8.479
SS	32.759	32.634	36.343
Be_{avg}	0.371	0.354	0.404

Table 9
Effects of the Carreau–Yasuda model parameter (m) on the average Nusselt and Sherwood numbers in different Rayleigh numbers at n = 1.5, $Cu = 1$, and Le = 2.5

	m= 1	m = 10	m = 100
Ra = 10^4			
Nu_{avg}	1.811	2.052	2.067
Sh_{avg}	3.210	3.695	3.715
Ra = 10^5			
Nu_{avg}	3.595	4.004	4.037
Sh_{avg}	6.031	6.624	6.670

Table 10
Effects of the Carreau–Yasuda model parameter (m) on different entropy generations and average Bejan number in different Rayleigh numbers at n = 1.5, $Cu = 1$, and Le = 2.5

	$m = 1$	$m = 10$	$m = 100$
Ra = 10^4			
ST	2.278	2.557	2.583
SF	1.108	1.307	1.323
SD	1.854	2.157	2.175
SS	5.176	5.957	6.016
Be_{avg}	0.777	0.766	0.765
Ra = 10^5			
ST	4.732	5.606	5.667
SF	24.252	30.572	30.923
SD	3.836	4.675	4.731
SS	32.759	40.792	41.261
Be_{avg}	0.371	0.373	0.374

Table 11
Effects of the Carreau number (Cu) on the average Nusselt and Sherwood numbers at Ra = 10^5, n = 1.5, $m = 1$, and Le = 2.5

	$Cu = 0.01$	$Cu = 0.1$	$Cu = 1$	$Cu = 10$	$Cu = 50$	$Cu = 100$
Nu_{avg}	4.026	3.928	3.595	3.036	2.666	2.521
Sh_{avg}	6.654	6.506	6.031	5.274	4.763	4.528

Table 12
Effects of the Carreau number (Cu) on different entropy generations and average Bejan number in different Rayleigh numbers at Ra = 10^5, n = 1.5, $m = 1$, and Le = 2.5

	$Cu = 0.01$	$Cu = 0.1$	$Cu = 1$	$Cu = 10$	$Cu = 50$	$Cu = 100$
ST	5.635	5.406	5.606	3.777	3.155	2.917
SF	30.660	28.883	30.572	18.862	15.479	14.168
SD	4.695	4.456	4.675	3.103	2.718	2.565
SS	40.930	38.684	40.792	25.679	21.290	19.587
Be_{avg}	0.374	0.374	0.373	0.358	0.353	0.354

List of Figures

Fig.12 Comparison of different local entropy generations for different Carreau numbers at Ra = 10^5, n = 1.5, $m = 1$, Le = 2.5, N = 0.1

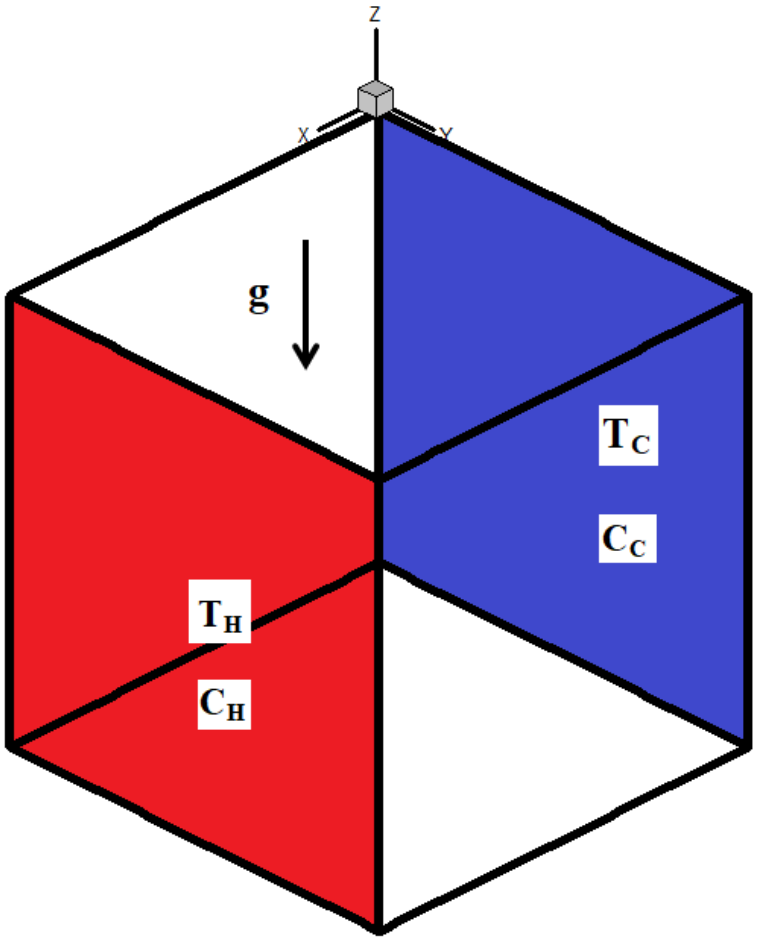

Fig. 1. Geometry of present study

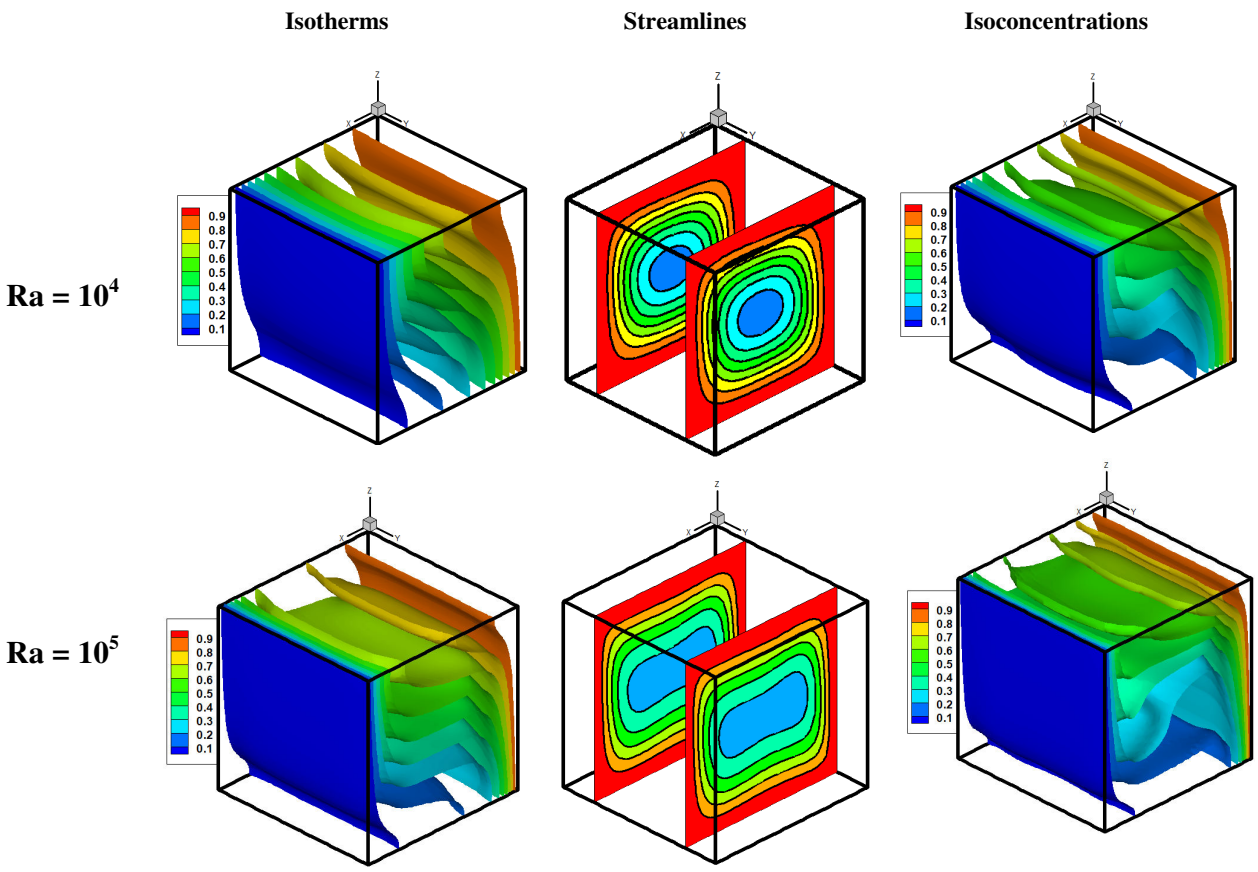

Fig. 2. Comparison of the isotherms, isoconcentrations, and streamlines for different Rayleigh numbers at n = 1.5, N = 0.1, $m = 1, Cu = 1$, Le = 2.5

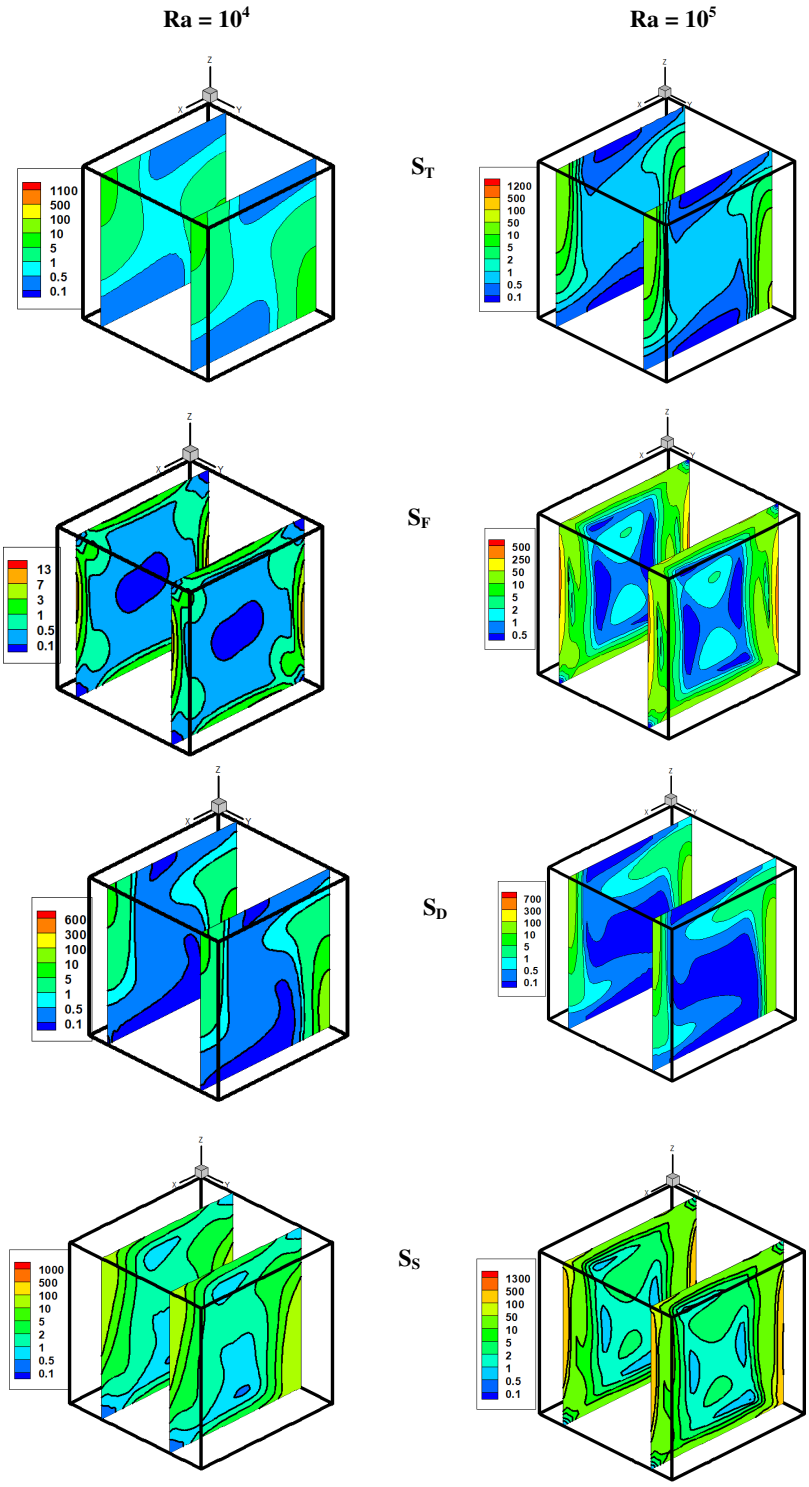

Fig. 3. Comparison of different local entropy generations for different Rayleigh numbers at n = 1.5, N = 0.1, Le = 2.5

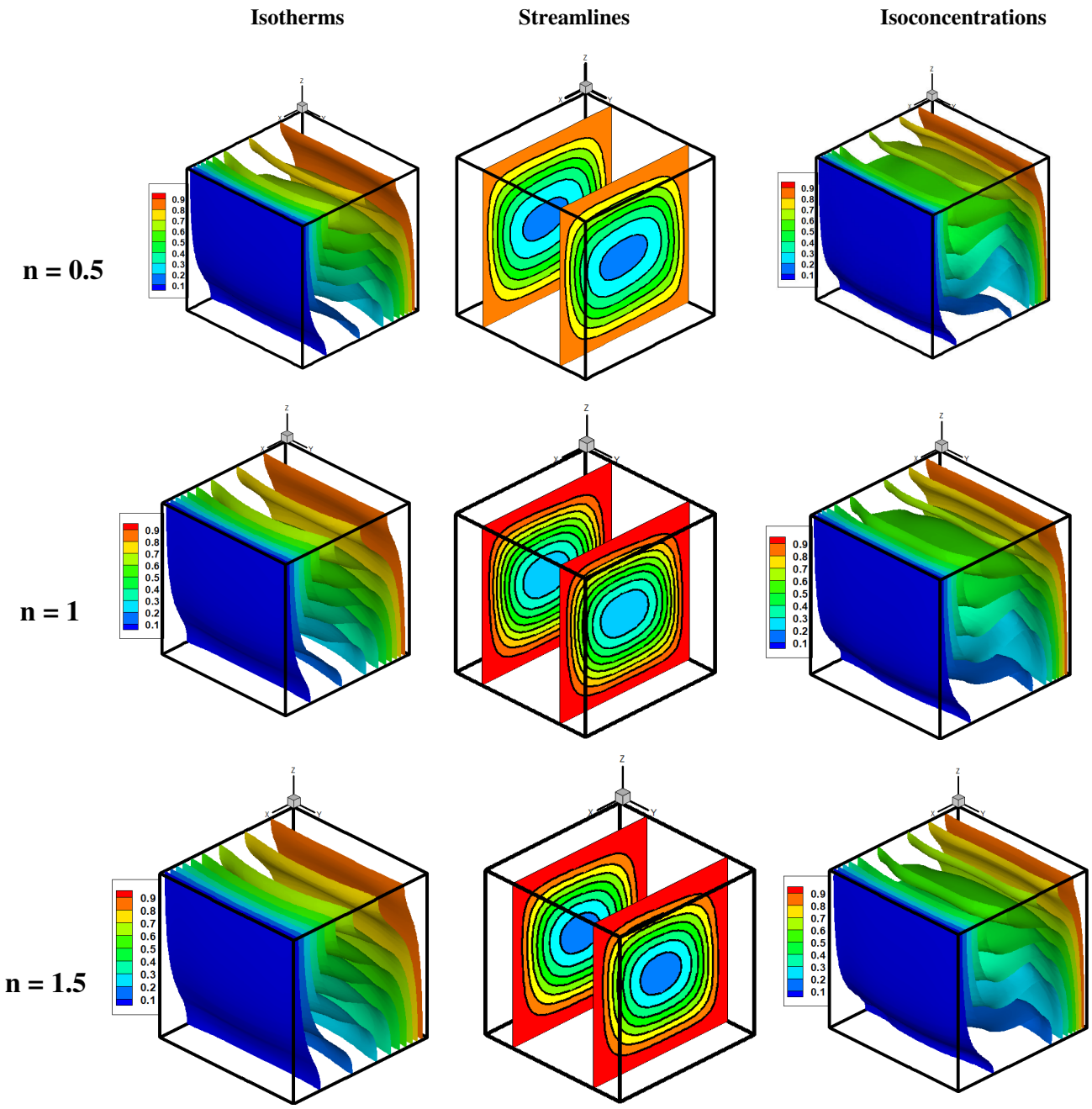

Fig. 4. Comparison of the isotherms, isoconcentrations, and streamlines for different power-law indexes at Ra $= 10^4$, N $= 0.1$, $m = 1, Cu = 1$, Le $= 2.5$

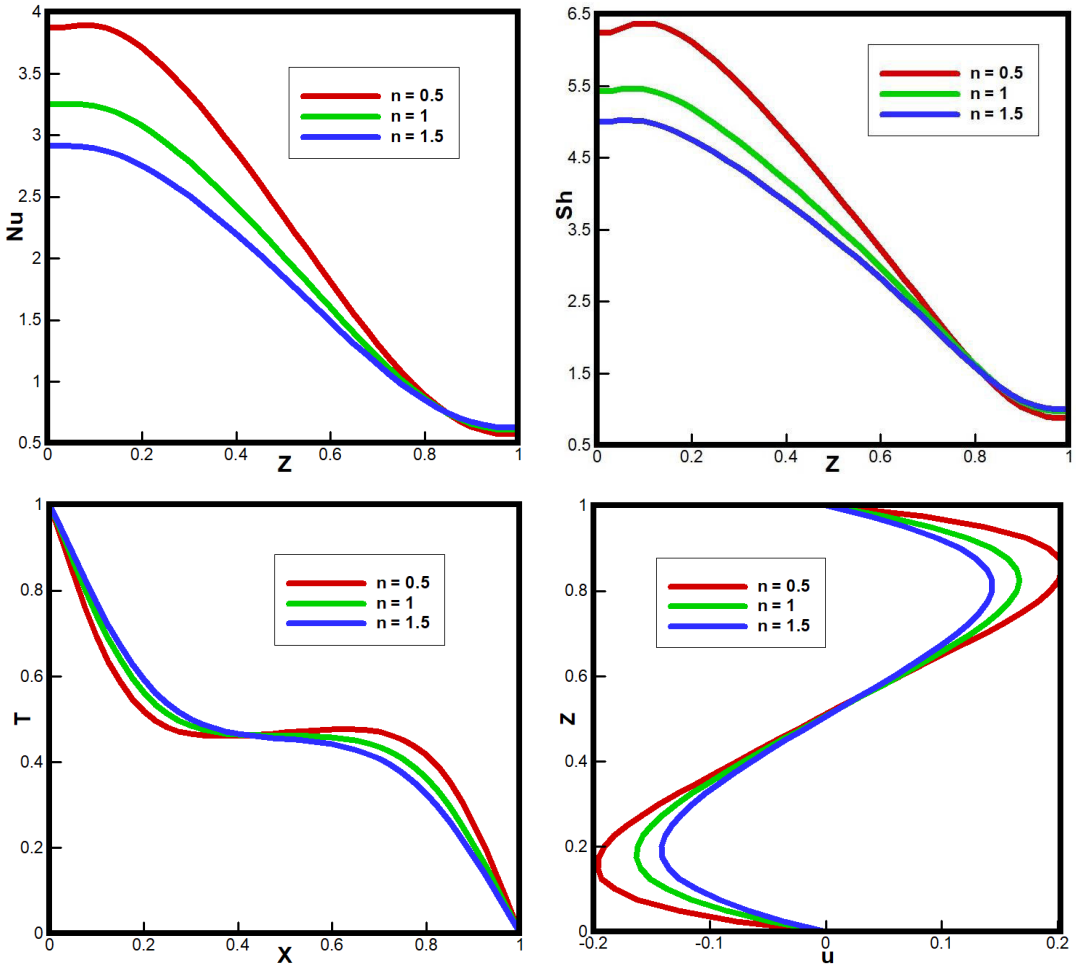

Fig. 5. Comparisons of local Nusselt and Sherwood numbers at $x = 0.5$, velocity and temperature distributions at $Z = 0.5$ on the hot left side wall, for different power-law indexes at Ra $= 10^4$, N $= 0.1$, $m = 1, Cu = 1$, Le $= 2.5$

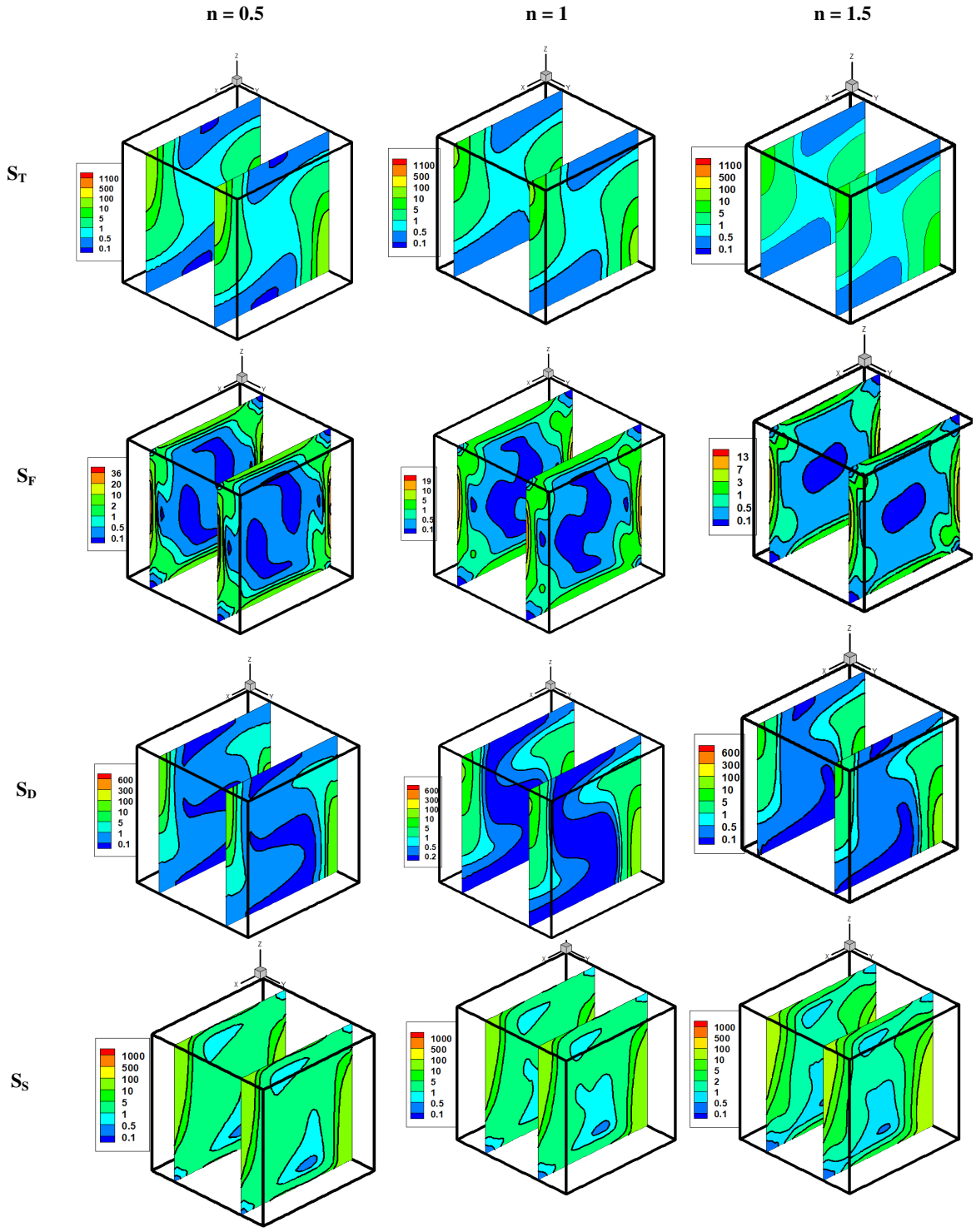

Fig. 6. Comparison of different local entropy generations for different power-law indexes at Ra = 10^4, N = 0.1, $m = 1, Cu = 1$, Le = 2.5

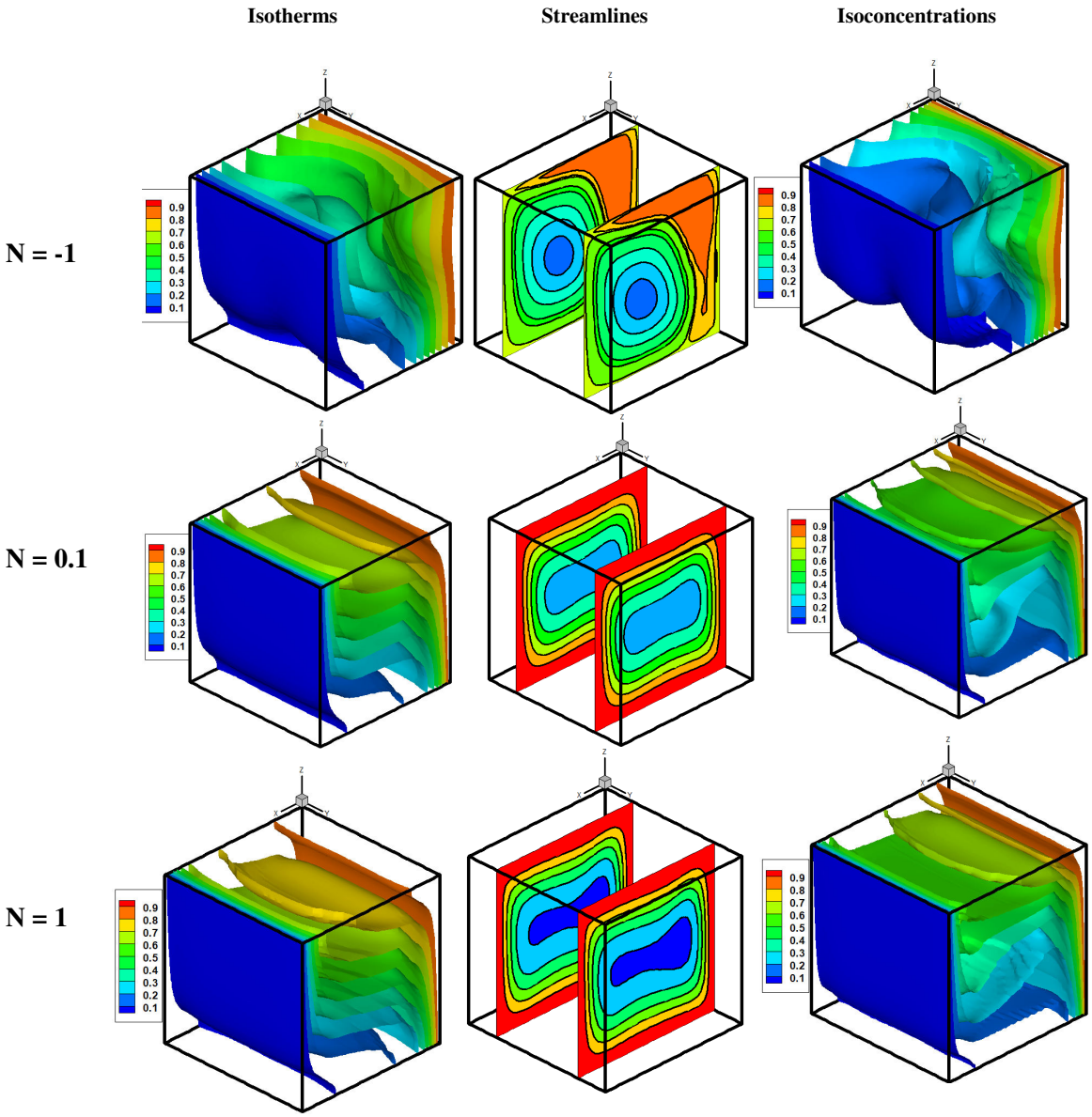

Fig. 7. Comparison of the isotherms, isoconcentrations, and streamlines for different buoyancy ratios at Ra = 10^5, n = 1.5, $m = 1, Cu = 1$, Le = 2.5

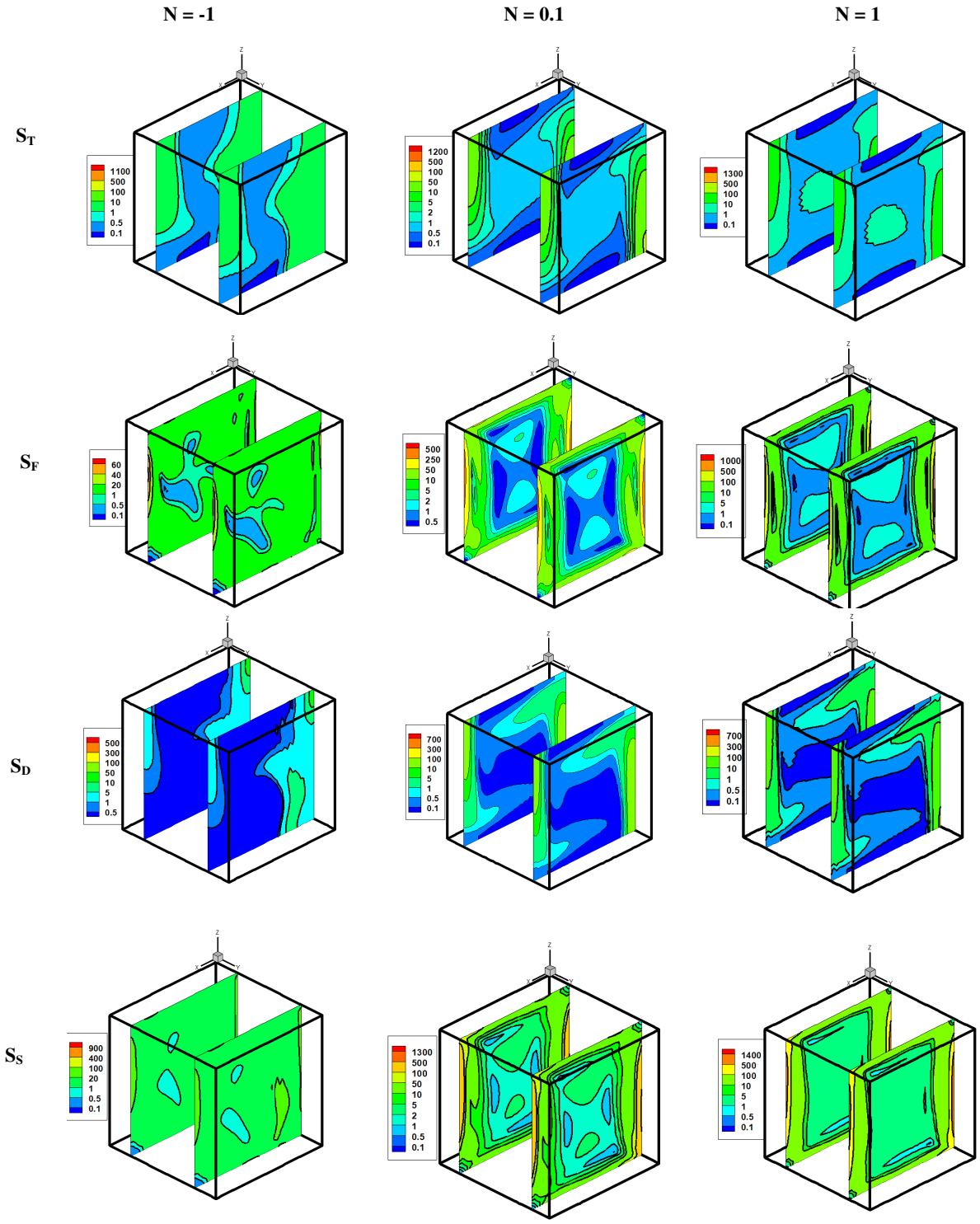

Fig. 8. Comparison of different local entropy generations for different buoyancy ratios at Ra = 10^5, n = 1.5, $m = 1, Cu = 1$, Le = 2.5

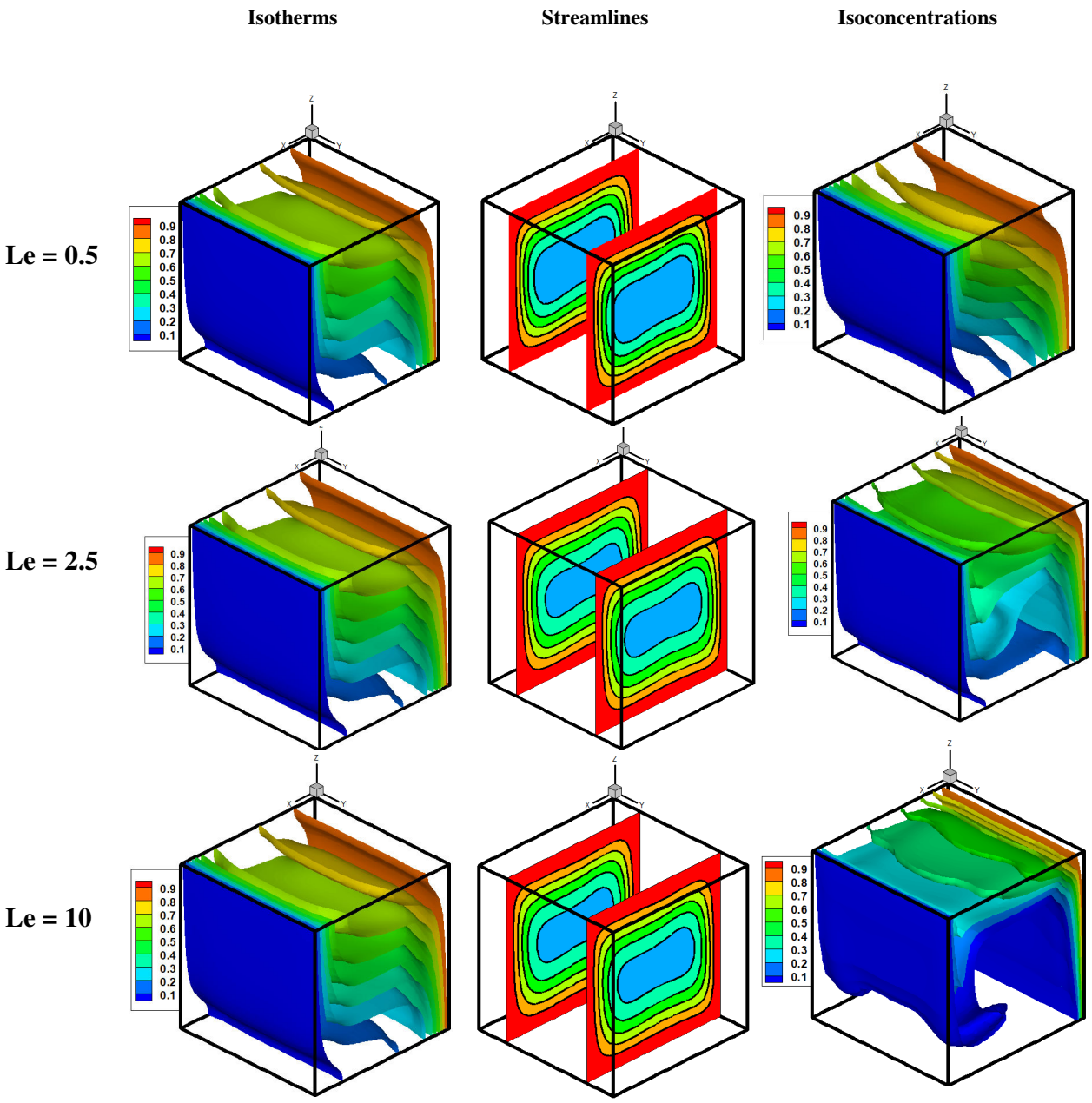

Fig. 9. Comparison of the isotherms, isoconcentrations, and streamlines for different Lewis numbers at Ra $= 10^5$, n $= 1.5$, $m = 1, Cu = 1$, N $= 0.1$

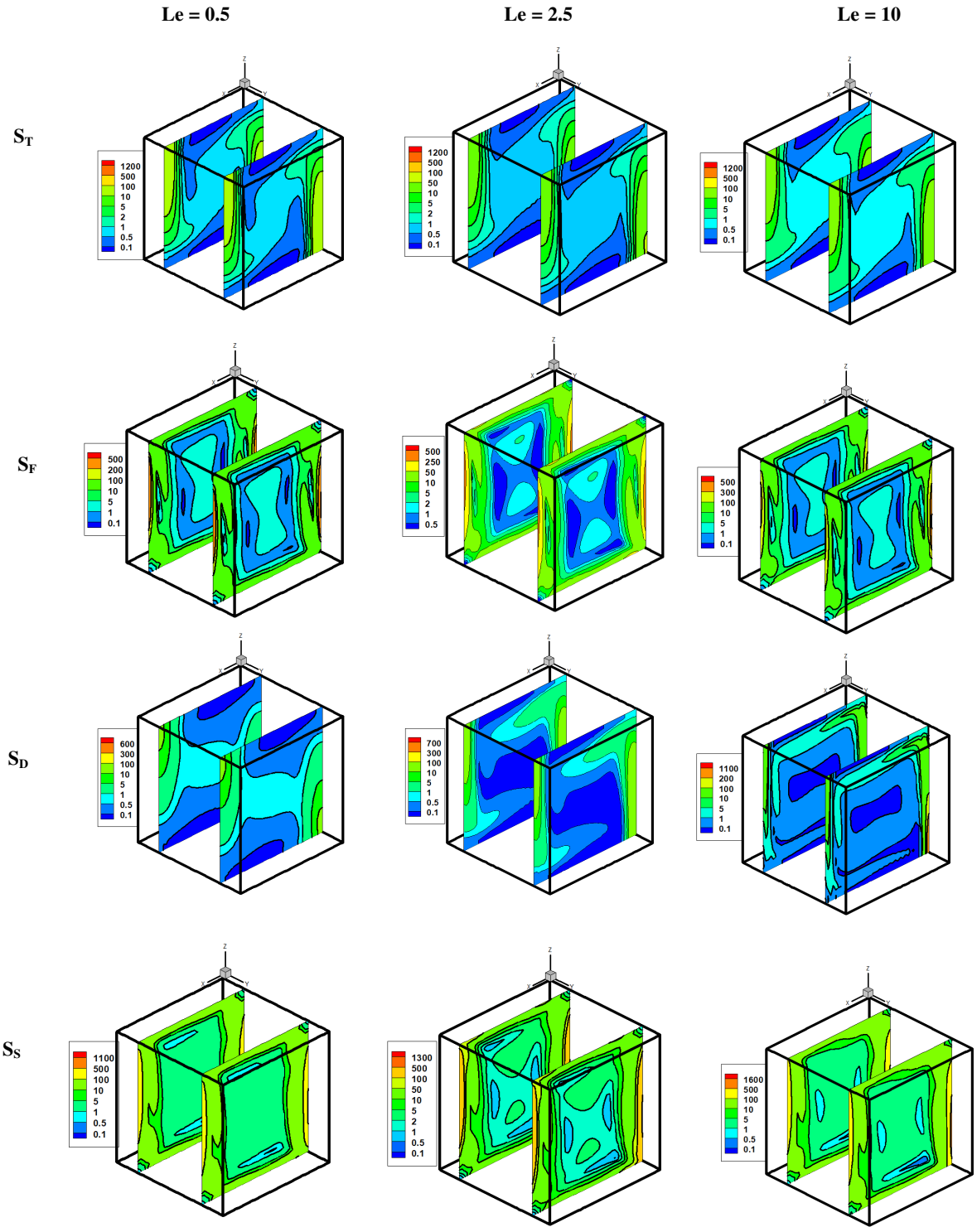

Fig. 10. Comparison of different local entropy generations for different Lewis numbers at Ra = 10^5, n = 1.5, $m = 1, Cu = 1$, N = 0.1

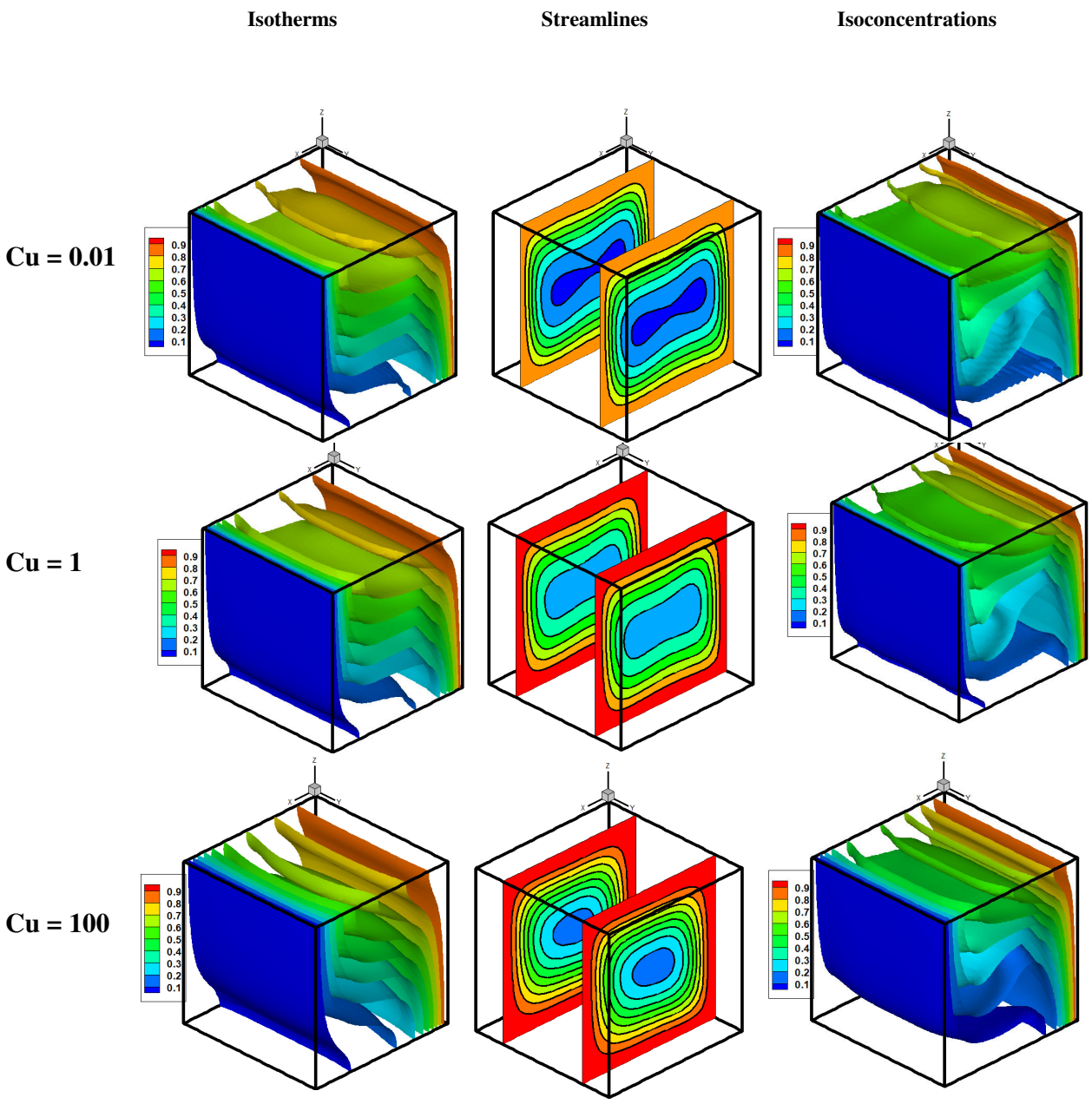

Fig. 11. Comparison of the isotherms, isoconcentrations, and streamlines for different Carreau numbers at Ra = 10^5, n = 1.5, $m = 1$, Le = 2.5, N = 0.1

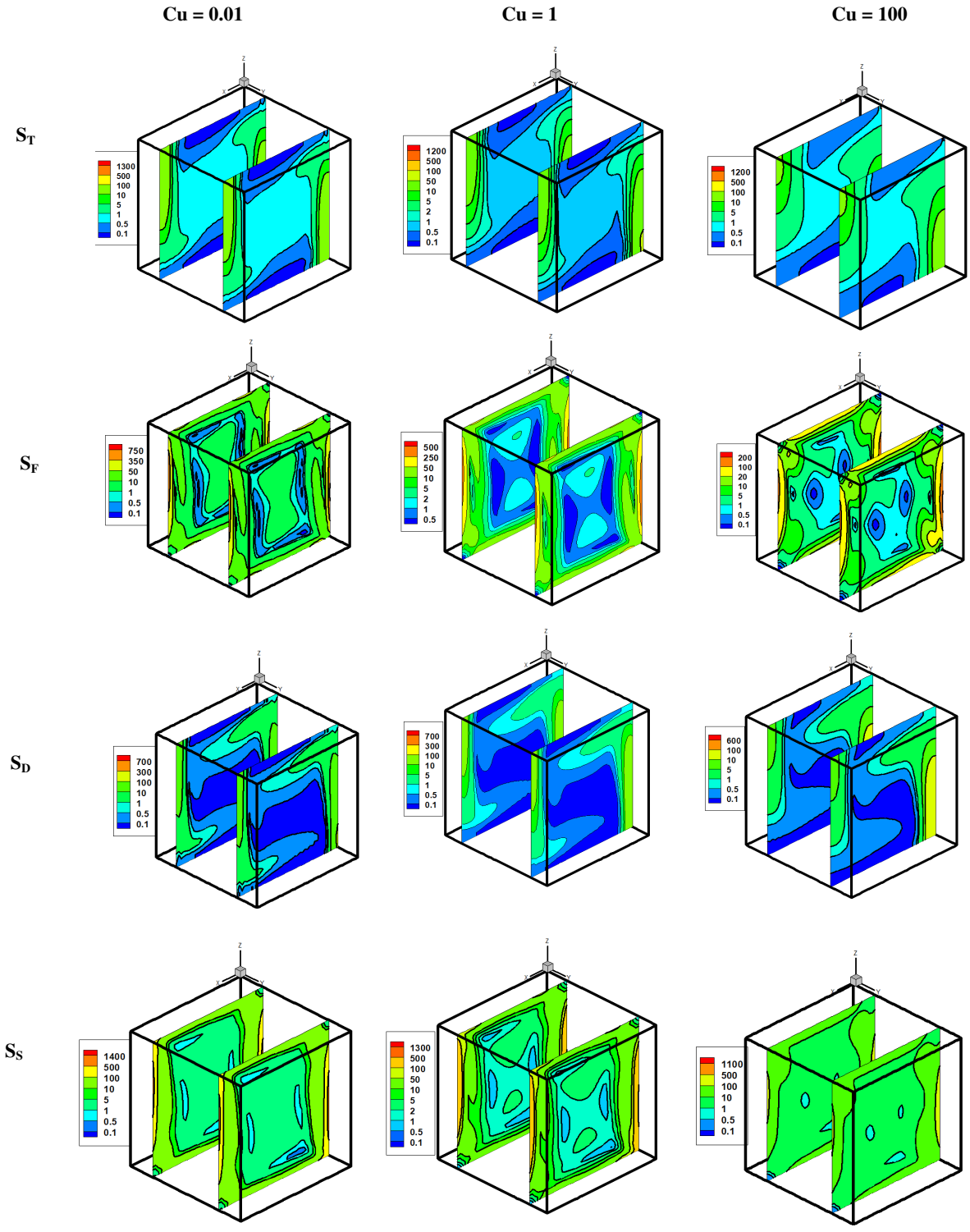

Fig. 12. Comparison of different local entropy generations for different Carreau numbers at Ra = 10^5, n = 1.5, $m = 1$, Le = 2.5, N = 0.1